Decoupling of $\Delta O_2/Ar$ and particulate organic carbon dynamics in near shore surface ocean waters

Sarah Z. Rosengard[1], Robert W. Izett[1], William J. Burt[2], Nina Schuback[3], and Philippe D. Tortell[1,4]

1. Department of Earth, Ocean and Atmospheric Sciences, University of British Columbia, Vancouver, V6T 1Z4, Canada
2. College of Fisheries and Ocean Sciences, University of Alaska Fairbanks, Fairbanks, 99775, USA
3. Institute of Geological Sciences and Oeschger Center for Climate Change Research, University of Bern, Bern, Switzerland
4. Department of Botany, University of British Columbia, Vancouver, V6T 1Z4, Canada

Correspondence to: Sarah Z. Rosengard (srosengard@eoas.ubc.ca)

Abstract. We report results from two Lagrangian drifter surveys off the Oregon coast, using continuous ship-board sensors to estimate mixed layer gross primary productivity (GPP), community respiration (CR), and net community production (NCP) from variations in biological oxygen saturation ($\Delta O_2/Ar$) and optically-derived particulate organic carbon (POC). At the first drifter survey, conducted in a nearshore upwelling zone during the development of a microplankton bloom, net changes in $\Delta O_2/Ar$ and [POC] were largely decoupled. Significant differences in GPP and NCP derived from $\Delta O_2/Ar$ ($NCP_{O2/Ar}$) and POC (NCP_{POC}) time series suggest the presence of large POC losses from the mixed layer. At this site, we utilized the discrepancy between $NCP_{O2/Ar}$ and NCP_{POC} and additional constraints derived from surface water excess nitrous oxide (N_2O) to estimate particle export and vertical mixing fluxes, respectively. At the second drifter survey, conducted in lower productivity, density-stratified offshore waters, we also observed significant discrepancies between $\Delta O_2/Ar$ and POC-derived GPP and CR rates. However, net [POC] changes were positively correlated with $\Delta O_2/Ar$ changes, yielding closer agreement in NCP estimates derived from these measurements. This suggests a tighter relationship between production and community respiration, and lower export rates. These results provide insight into the possibilities and limitations of estimating productivity from continuous underway POC and $\Delta O_2/Ar$ data in contrasting oceanic waters. Our observations support the use of diel POC measurements to estimate NCP in lower productivity waters with limited vertical carbon export, and the potential utility of coupled O_2 and optical measurements to estimate the fate of POC in high productivity regions with significant POC export.

1 Introduction

Marine primary productivity provides the major source of organic carbon to the ocean, supporting the vast majority of marine ecosystem biomass. On short time scales, a large fraction of this fixed organic carbon is converted back to CO_2 through community respiration (CR). The difference between gross primary productivity (GPP) and CR – net community production (NCP) – sets an upper limit on the quantity of particulate organic carbon that can be exported out of the mixed layer as sinking particles, transferred to the dissolved organic carbon (DOC) pool, or consumed by upper trophic levels. Accurate assessment of NCP is thus critical to

47 understanding trophic balance and the fate of organic carbon in the surface ocean. Because
48 traditional incubation-based approaches to quantify GPP, net primary productivity (NPP) and CR
49 are labor-intensive and error prone (Gieskes et al., 1979; Fogg and Calvario-Martinez, 1989;
50 Marra, 2009; Quay et al., 2010), NCP remains challenging to quantify on ecologically-relevant
51 time and space scales.
52 In recent years, automated *in situ* measurements of seawater optical properties have been
53 increasingly used to estimate gross and net primary productivity from changes in optically-
54 derived surface water POC concentrations (e.g., Graff et al., 2016; Burt et al., 2018). This
55 approach is based on the relationship between POC concentrations and the particulate fraction of
56 the beam attenuation coefficient (c_p) (Siegel et al., 1989; Stramska and Dickey, 1992; Gardner et
57 al., 1993; Claustre et al., 1999; Gernez et al., 2011), which can be used to resolve diurnal
58 variations in POC. This diurnal variability results from the daytime accumulation of
59 photosynthetically-produced organic carbon, and nighttime loss of fixed carbon through
60 community respiration, and can thus be used to infer NCP on daily time-scales. The accuracy of
61 this approach depends on the key assumption that variations in c_p capture most of the variability
62 in POC concentration, and it has been shown that beam attenuation is most sensitive to particles
63 with a diameter range of 0.5–20 µm (Stramski and Kiefer 1991; Marra, 2002; Claustre et al.,
64 2008). To date, most efforts to calculate daily NCP from c_p variability have focused on low
65 productivity offshore regions, where particle sizes are small and POC losses like particle export
66 are limited (Claustre et al., 2008; White et al., 2017). These studies have reported good
67 agreement between optically-derived GPP estimates and independent estimates of NPP from ^{14}C
68 incubations (White et al., 2017), suggesting a tight coupling between primary productivity and
69 mixed layer POC dynamics over daily time scales.
70 Another approach to NCP quantification is based on autonomous measurements of
71 surface water dissolved oxygen to argon ratios (O_2/Ar). Argon normalization is used to correct
72 for any physically-induced changes in O_2 saturation, such that the derived saturation anomaly,
73 ΔO_2/Ar, is a tracer of net biological O_2 production (Kaiser et al., 2005; Tortell, 2005; Cassar et
74 al., 2009). At steady-state, and in the absence of significant lateral advection and vertical mixing,
75 the sea-air flux of excess biologically-produced O_2 is equivalent to NCP. With the development
76 of automated ship-board mass spectrometers, there has been a significant increase in surface
77 water O_2/Ar measurements, and these have been used to examine O_2 variability resulting from

diurnal variations of photosynthesis and respiration, and to infer NCP in a variety of oceanic ecosystems (Reuer et al., 2007; Stanley et al., 2010; Tortell et al., 2011, 2014; Hamme et al., 2012; Nicholson et al., 2015; Manning et al., 2017). Recent efforts have shown that NCP estimates from $\Delta O_2/Ar$ measurements can be corrected for vertical mixing using water column N_2O measurements as a tracer (Cassar et al. 2014; Izett et al. 2018), but application of this methodology must assume that lateral advection is negligible.

Combined measurement of mixed layer POC and O_2 dynamics holds the potential to better constrain surface water carbon budgets in biogeochemically dynamic regions, like upwelling zones, at high spatial and temporal resolution. In net autotrophic systems, an increase in $\Delta O_2/Ar$ reflects the accumulation of excess photosynthetic O_2 in the mixed layer, but provides no direct insight into the fate of the resulting organic carbon. In the absence of particle export, grazing or DOC production, an increase in $\Delta O_2/Ar$, corrected for air-sea exchange and vertical mixing, should be matched by a parallel increase in POC accumulation measured by optical sensors. By comparison, high POC export, DOC production or grazing coupled to vertical migrations would act to decouple $\Delta O_2/Ar$ from optically-derived POC measurements in the mixed layer.

In previous studies, authors have used simultaneous O_2 and c_p measurements on moorings to describe mixed layer O_2 and POC dynamics in various marine environments (Stramska and Dickey, 1992; Kinkade et al., 1999; Dickey and Chang, 2002). However, few studies to date have compared estimates of primary productivity from simultaneous measurements on daily time scales. Briggs et al. (2018) and Alkire et al. (2012) were the first to explicitly combine concurrent measurements of O_2 and POC from *in situ* autonomous sensors to quantify mixed layer productivity during a ~2-month Lagrangian study of the 2008 North Atlantic spring bloom. Tracking daily changes in mixed layer O_2 and POC concentrations, Alkire et al. (2012) constructed a detailed budget of surface ocean organic carbon throughout the course of the bloom, using the difference between O_2-based NCP and net POC accumulation to assess the partitioning of NCP into different carbon pools (sinking particles, phytoplankton biomass, and DOC). Building on this work, Briggs et al. (2018) examined the role of respiration, particle export, and DOC production in decoupling O_2 and POC dynamics through different bloom stages, demonstrating significant differences between GPP estimates derived from O_2, beam

attenuation, and backscatter measurements. To our knowledge, such a detailed examination of O_2 and POC dynamics has not been reported for other marine systems.

Here, we present new results from a field study of diel variability in $\Delta O_2/Ar$ and optical properties in two contrasting near-shore regions of the Subarctic North Pacific. Using ship-board automated sensors deployed along a Lagrangian drifter track, we resolved fine-scale temporal patterns in biological oxygen production and POC concentration in a high productivity coastal upwelling zone over the continental slope and in lower productivity stratified waters offshore. The biogeochemical differences between both sites provided a unique opportunity to compare GPP, CR and NCP estimates derived from $\Delta O_2/Ar$ and POC in contrasting trophic regimes. We expected to observe significant differences between $\Delta O_2/Ar$ and POC-derived GPP, CR, and NCP estimates in the higher productivity site, reflecting greater carbon export capacity and DOC production. By comparison, we hypothesized that discrepancies in these rates would be smaller at the lower productivity site, reflecting a tighter coupling between O_2 and POC dynamics.

The results of this investigation have extended findings from the 2008 North Atlantic bloom to a high productivity coastal upwelling environment, expanding comparisons of GPP, CR and NCP derived from daily $\Delta O_2/Ar$ and POC variations to a region where vertical mixing fluxes significantly influence the surface water mass balance. These dynamic systems play a disproportionately important role in marine biogeochemical cycling, but they pose significant challenges for interpreting time series of ecosystem metabolism. Furthermore, our study results further expand applications of a recent field approach to correcting NCP for vertical mixing (Izett et al., 2018), suggesting that this approach has significant merit in reconstructing productivity estimates from a variety of mixed layer tracers. We discuss the implications of our coupled O_2-POC measurements for understanding biological carbon cycling in coastal marine waters, and suggest additional approaches to further improve the utility of coupled $\Delta O_2/Ar$ and optically-derived organic carbon measurements for evaluating the fate of marine primary productivity across marine trophic gradients.

2 Methods

2.1 Field site and Lagrangian surveys

Field studies were conducted on board the R/V *Oceanus* in August 2017, during a transect through the Northeast Subarctic Pacific Ocean. Two Lagrangian drifters were deployed off the Oregon coast, allowing us to track diurnal patterns in phytoplankton productivity and particulate organic carbon cycling in two distinct water masses (Fig. 1). Underway temperature and salinity measurements, collected by a Seabird SBE 45 thermosalinograph, as well as satellite (Aqua MODIS) and ship-based chlorophyll-a (Chl-a) observations, were used to guide the specific location and timing of the drifter deployments. Drifter 1 was deployed on 20 August 2017 (~9:30 PDT), ~40 km from the Oregon coast (44.54° N, 124.58° W), in the vicinity of an upwelling feature detected based on low sea surface temperature, and elevated salinity and [Chl-a]. The drifter, consisting of a beacon, GPS transmitter and 5 m drogue, was recovered at ~18:30 on 23 August 2017 (44.40° N, 124.55° W) for a total deployment of 3 days and 9 hours. Upon recovery, the drogue was missing, implying the potential for some erratic sub-surface drifting (discussed below). Drifter 2 was deployed approximately 200 km from shore (43.75° N, 126.50 °W) in a relatively warm and low salinity water mass, with low Chl-a concentrations. This second drifter was deployed at ~07:45 on 24 August 2017, and was recovered after 2 days and six hours at ~14:00 on 26 August 2017 at 43.80° N, 126.99° W. Because the *Oceanus* lacks a dynamic positioning system, the ship was not always able to perfectly track the drifter locations. To correct for these positional offsets, we discarded any observations obtained when the ship was more than 1.5 km away from the drifter location. This filtered dataset resulted in measurements every ~15 minutes during the two drifter deployments, yielding 325 and 218 quality-controlled underway observations for drifters 1 and 2, respectively.

2.2 Underway measurements

Continuous underway measurements of surface seawater optical properties were collected using Seabird (formerly Wetlabs) ECO-BB3 and ac-s sensors, following the methods outlined in detail by Burt et al. (2018). Water was collected from the ship's seawater supply system with a nominal intake of 5 m depth. Our instrument package included fully automated data collection, and hourly filtered blanks (0.2µm), which provided measurements of dissolved seawater optical properties used to infer particulate absorption (a_p) and beam attenuation (c_p) at 82 wavelengths between 400 and ~735 nm, and backscatter (b_{bp}) at 470 nm, 532 nm, and 650

nm. The BB-3 and ac-s measurements were binned into 1-minute intervals. Prior to binning, the absorption and beam attenuation data were first sub-sampled every 50 data acquisition cycles (~12.5 seconds) to enable faster processing time. The optical measurements were accompanied by continuous surface photosynthetically active radiation (PAR) and windspeed data obtained from a Biospherical QSR-220 PAR sensor and Gill WindObserver II ultrasonic wind sensor mounted on the ship's bow.

Chlorophyll-a (Chl-a) concentrations were derived from the particulate absorption line height at 676 nm (a_{LH}) (Roesler and Barnard, 2013). Five-minute match-ups between underway a_{LH} and discrete filtered [Chl-a] measurements from the entire cruise transect (Sect. 2.4) were used to derive a best fit coefficient for the linear relationship between a_{LH} and [Chl-a] (r^2=0.87, n= 58, $p<0.01$). Particulate organic carbon (POC) concentrations (µg/L) were derived from particulate beam attenuation at 660 nm ($c_{p,660}$), using the empirical model in Graff et al. (2015). Similarly, phytoplankton organic carbon (C_{ph}) concentrations were calculated, using an empirical relationship between particulate backscatter at 470 nm ($b_{bp,470}$) and [C_{ph}] in µg/L (Graff et al., 2015). We used a limited set of 5m discrete measurements (n=6) to evaluate the relationship between POC concentrations and c_p at 660nm, and the applicability of the Graff et al. (2015) model to our observations. As shown in Fig. S1, the POC measurements were significantly correlated to c_p (r^2=0.88, $p<0.05$), with a slope and intercept of 391.6 ± 201.6 and 36.7 ± 79.1, respectively. This slope was not significantly different from that of the Graff et al. algorithm (419.8) although our y-intercept was higher. Notwithstanding the relatively small number of discrete POC samples, and some scatter around the regression line, the similarity of our POC-c_p calibration to that reported by Graff et al. (2015) suggests that our optically-derived POC estimates are reasonably robust.

To obtain information on the particle size spectrum, we derived the wavelength-dependent slope of particulate backscatter by fitting the three b_{bp} coefficients (470 nm, 532 nm, 650 nm) to an exponential equation (Stramska et al., 2003; Loisel et al., 2006; Kostadinov et al., 2009). Finally, to assess interference of inorganic minerals on POC, and C_{ph} variability, we calculated the wavelength-specific bulk refractive index (η_p) from backscatter/total scatter ratios ($\frac{b_{bp}}{c_p - a_p}$) and the wavelength-dependent c_p slope, following the approach of Boss et al. (2001), Twardowski et al. (2001) and Sullivan et al. (2005).

In addition to optical measurements, the seawater biological oxygen saturation anomaly ($\Delta O_2/Ar$) was measured at ~20 second resolution using a membrane inlet mass spectrometer connected to the ship's seawater intake. The seawater ratio of dissolved O_2 and Ar was determined by diverting a continuous flow of water across a dimethylsilicone membrane interfaced with a Hiden Analytical HAL20 triple filter quadropole mass spectrometer. The O_2/Ar ratio of air-equilibrated standards ($[O_2/Ar]_{eq}$), incubated at ambient sea surface temperature, was measured every two hours. Values of $\Delta O_2/Ar$ were thus calculated as the percent deviation of seawater O_2/Ar measurements from the air-equilibrated ratio, using $\Delta O_2/Ar = 100\% * ([O2/Ar]_{meas} / [O_2/Ar]_{eq} - 1)$ (Tortell, 2005; Tortell et al., 2011).

2.3 Mixed layer depth

Over the course of both drifter deployments, we conducted regular hydrographic casts (every six to ten hours) to examine depth profiles of seawater hydrography and biogeochemical variables. Temperature, salinity, dissolved O_2 concentrations and Chl-a fluorescence profile data from the CTD casts were measured by a Seabird-SBE 38 temperature sensor, Seabird-SBE 4 conductivity sensor, SBE 43 dissolved O_2 sensor, and a Seabird ECO fluorometer, respectively, and binned into 1 m intervals. Vertical profiles at the drifter 1 site showed relatively weak density stratification, likely as a result of recent upwelling. For this reason, we estimated mixed layer depths (z_{mld}) based on visible inflection points in the dissolved $[O_2]$, fluorescence and density profiles, assuming that dissolved O_2 concentrations and fluorescence are relatively uniform in the mixed layer. Within a single CTD cast, mixed layer depths varied by up to 28% across all three profile measurements. The [Chl-a] fluorescence profiles had the most well-defined inflection points, and we thus used these data to estimate z_{mld} at all casts. Excluding fluorescence profiles from the first day (Sect. 3.1), and two casts at 6am and midnight on second and third 24-hour intervals, respectively, which displayed relatively noisy density profiles, an average z_{mld} value (19 ± 2 m) was derived and applied to all subsequent analyses.

In comparison to the drifter 1 site, CTD cast profiles during drifter deployment 2 showed larger density gradients. We thus computed z_{mld} using a density difference criterion of 0.25 kg/m_3 (Thomson et al., 2003; de Boyer Montégut et al., 2004) from median values within the upper-most 4–6 m of the profile. We found that this critical density criterion was necessary to

capture the depth of inflection in O_2 and [Chl-a]. In all CTD casts except one, density difference-based z_{mld} values were within 5 meters of the values derived from the inflection points on density profiles. An average z_{mld} value estimated from the density-difference approach (22 ± 5 m) was applied to all subsequent analyses.

2.4 Discrete samples

Concentrations of phosphate ([PO_4^{3-}]), dissolved silica ([SiO_2]), and nitrate and nitrite ([$NO_3^- + NO_2^-$], were measured in seawater samples collected from daily Niskin bottle casts. Following collection, nutrient samples were filtered through 0.2 µm pore polycarbonate membranes and immediately frozen at -80°C on board the ship. These samples were stored at -20°C until subsequent colorimetric laboratory analyses (Murphy and Riley, 1962; Riley, 1977) with a Lachat QuikChem 8500 Series 2 Flow Injection Analysis System.

Concentrations of dissolved oxygen (O_2) and nitrous oxide (N_2O) were measured in discrete samples collected in Niskin bottles during both drifter deployments (Fig. S2), following methods outlined in (Capelle et al., 2015). These N_2O measurements were used to correct NCP estimates for vertical mixing (see Sect. 2.6), following the approach described by Cassar et al. (2014) and Izett et al. (2018). Profile samples from the first day of drifter deployment 1 (August 20) were omitted from calculations, as underway surface temperature and salinity measurements indicated intrusion of an external water mass (further discussed in Sect. 3.1) (Fig. S3). Three profiles collected from 12:00 (PDT) CTD casts during the following three days of the deployment (August 21, 22 and 23) were applied to the NCP mixing correction at drifter station 1 (Sect. 2.6.1).

Surface (~5 m) discrete seawater samples were collected either from Niskin bottles or from the ship's surface seawater intake system for HPLC analysis of Chl-a concentrations and other phytoplankton pigments. Single or duplicate samples were filtered onto 25 mm GF/F filters, flash-frozen in liquid nitrogen, and stored at -80°C until analysis, following the methodology described in Schuback et al. (2016). Additional samples were collected from the seawater intake for size-fractionated Chl-a analysis (Zeng et al., 2018). These samples were filtered through stacked 47 mm filters (0.2 µm, 2 µm and 20 µm pore size) separated by a mesh

spacer. Filtered samples were extracted in 5 mL of 90% acetone at 4°C until analysis within 24–48 hours using a Turner Trilogy Fluorometer on board the ship.

Discrete samples for POC analysis were collected at two depths from several CTD casts. Surface samples were collected at both drifter sites from 5 m depth, while deeper samples were collected at near the base of the euphotic zone (~1% PAR), corresponding to 40–60 m at drifter site 1, and 100–120 m at drifter site 2. POC samples (~1–4 L) were filtered through a pre-combusted (450 °C) Whatman GF/F filter (nominal pore size ~ 0.7 μm), and stored at -80°C until laboratory analysis. Prior to analysis, samples were thawed and dried at 50°C overnight, fumigated with concentrated hydrochloric acid for 48 hours, and dried again at 50°C overnight. POC concentrations in samples (and blank combusted filtered treated as described above) were quantified using an *Elementar* vario MICRO cube CHNS analyzer. Blank-corrected discrete POC concentrations were used to validate application of the [POC] model in Graff et al. (2015) to our underway c_p data (Sect. 2.2; Fig. S1).

2.5 Net Primary Productivity

Daily-integrated net primary productivity (NPP) was calculated in two ways. First, carbon uptake was determined from 24-hour ^{14}C-incubations with 5 m triplicate seawater samples collected from early morning CTD casts. Measurements were made on two different mornings during drifter deployment 1 and on one morning during drifter deployment 2. The measurements were conducted following the protocol outlined in Hoppe et al. (2017). Depth-integrated NPP was calculated by multiplying the derived 24-hour volumetric carbon fixation rate by the average mixed layer depth for the respective drifter period.

Second, daily-integrated net primary productivity was also estimated as a product of [C_{ph}] values derived from b_{bp}, and phytoplankton growth rates according to the carbon-based productivity model (CbPM) (Behrenfeld et al., 2005; Westberry et al., 2008; Graff et al., 2016; Burt et al., 2018). In these calculations, daily-averaged [C_{ph}], [Chl-a]/[C_{ph}], and mixed layer irradiance (E_g) calculated from the MODIS-derived surface PAR matched to drifter location were used to calculate growth rates and NPP every 24 hours. Chlorophyll-a concentrations were derived from absorption line height (Sect. 2.2), [C_{ph}] values from b_{bp}, and light extinction

coefficients (K_d) obtained from [Chl-a] to calculate E_g (Morel et al., 2007). An average mixed layer depth for each drifter period was applied to estimate mixed layer NPP (Sect. 2.3).

2.6 Quantification of GPP, CR and NCP

Gross primary productivity (GPP), community respiration (CR) and net community production (NCP) rates were calculated based on linear regressions of $\Delta O_2/Ar$ and POC against time over subsequent day (D) and night (N) intervals during both drifter deployments. Daytime was defined as the period during which PAR levels exceeded 20 µmol quanta $m^{-2}s^{-1}$. The average length of the day-time period was 13.6 ± 0.14 hours over the two drifter deployments. In the following sections, t_d represents the day length normalized to 24 hours, and t_n analogously represents the fractional night length, equivalent to 1-t_d. All daily rates were integrated through the mixed layer using the average z_{mld} for each drifter period, as described in Sect. 2.3.

2.6.1 O_2/Ar-derived rates

Quantification of $GPP_{O2/Ar}$, $CR_{O2/Ar}$, and $NCP_{O2/Ar}$ rates from diurnal cycles in $\Delta O_2/Ar$ (Ferrón et al., 2015) requires corrections for gas exchange and, potentially, vertical mixing fluxes. For these calculations, we first computed the rate of change in $\Delta O_2/Ar$ (dO_{2Bio}/dt) using linear regression analysis within successive daytime or nighttime intervals. We then derived estimates for the air-sea gas exchange (J_{ex}) and vertical mixing fluxes (F_{mix}) over the respective day or night interval to isolate the NCP contribution to observed $\Delta O_2/Ar$ changes (Izett et al., 2018; Tortell et al., 2014). Net O_2 production rates were converted into carbon units using a photosynthetic quotient (PQ) for new production of 1.4 for drifter period 1 calculations and a PQ for regenerated production of 1.1 for drifter period 2 (Laws, 1991). We assumed that CR rates were constant over each respective day length period (i.e. t_d + t_N).

$$NCP_{\frac{O_2}{Ar},D\ or\ N} = z_{mld}\left.\frac{dO_{2bio}}{dt}\right|_{D\ or\ N} + J_{ex}|_{D\ or\ N} + F_{mix} \quad (1)$$

$$GPP_{O2/Ar} = \frac{t_d(NCP_{\frac{O_2}{Ar},D} - NCP_{\frac{O_2}{Ar},N})}{PQ} \quad (2a)$$

$$CR_{O2/Ar} = \frac{NCP_{\frac{O2}{Ar},N}}{PQ} \quad (2b)$$

$$NCP_{\frac{O2}{Ar},24hr} = \frac{t_d NCP_{\frac{O2}{Ar},D} + t_N NCP_{\frac{O2}{Ar},N}}{PQ(t_d + t_N)} \quad (2c)$$

$$O_{2bio} = \Delta\frac{O_2}{Ar}\frac{1}{100\%}O_{2eq} \quad (3)$$

$$J_{ex} = k_{o2}O_{2bio} \quad (4)$$

$$F_{mix,O2/Ar} = k_{mix}\frac{dO_{2bio}}{dz} = k_{N2O}N_2O_{bio}\frac{dO_{2bio}}{dN2O_{bio}} \quad (5)$$

$$k_{mix} = k_{N2O}N_2O_{bio}(\frac{dN2O_{bio}}{dz})^{-1} \quad (6)$$

$$N_2O_{bio} = N_2O_{meas} - N_2O_{eq} - N_2O_{thermal} \quad (7)$$

Equilibrium concentrations of O_2 and N_2O ($[O_2]_{eq}$ and $[N_2O]_{eq}$) were calculated using the salinity and temperature-dependent equations of Garcia and Gordon (1992) and Weiss and Price (1980), respectively, and sea surface temperature and salinity from the ship's thermosalinograph. Estimates of surface excess N_2O saturation, $[N_2O]_{bio}$, included a heat flux correction to account for solubility changes (Keeling and Shertz, 1992; Jin et al., 2007; Izett et al., 2018). Non-weighted piston velocities (k_{O2} and k_{N2O}) were calculated using the diffusive air sea gas flux and Schmidt number parameterizations of Wanninkhof (2014) and Raymond et al. (2012), and ship-based wind speed data 10 m above the sea surface. Daytime and nighttime estimates for the gas exchange term, J_{ex}, were calculated using day/night average $[O_2]_{eq}$, $\Delta O_2/Ar$, and k_{O2} values. Vertical gas gradients ($\frac{dN2O_{bio}}{dz}$ and $\frac{dO_{2bio}}{dN2O_{bio}}$) were estimated from our measurements over the upper 100 m of the water column, following Izett et al. (2018).

At drifter site 1, daily F_{mix} values were calculated using daily $[N_2O]_{bio}$, daily vertical gradient and daily average k_{N2O} values (Sect. 2.4). Denitrification should not have been a source of N_2O within the upper 100 m of the water column because measured O_2 concentrations were consistently greater than the threshold value of ~50 mmol m^{-3} (e.g., Hopkinson and Barbeau,

2007). Likewise, we assumed no lateral advection of N_2O into drifter site 1, as there were little differences in the mixing ratio $[O_2]_{bio}/[N_2O]_{bio}$ across profile measurements (Fig. S2). While the August 22 CTD cast did exhibit a more anomalous $[O_2]_{bio}/[N_2O]_{bio}$ profile relative to the other two cast profiles, inclusion of these data had little impact on the vertical mixing correction. At drifter site 2, we assumed that vertical mixing was negligible due to the presence of strong density stratification, and therefore did not calculate a mixing flux correction at this site. In any case, the presence of a sub-surface O_2 maximum (Fig. S2) would significantly limit the application of the N_2O correction (Izett et al., 2018).

2.6.2 Optically-derived rates

We used the approach of Claustre et al. (2008) and White et al. (2017) to calculate daily-integrated GPP_{POC}, CR_{POC}, and NCP_{POC} from daytime and nighttime changes in POC (dPOC/dt), derived from linear regressions of POC concentrations against time through day and night intervals. In certain ocean environments, NCP_{POC} will not equate to $NCP_{O2/Ar}$ as a result of additional POC sinks, including export, grazing and DOC production. Under these conditions, CR_{POC} includes these loss term, and therefore NCP_{POC} more accurately reflects net POC accumulation. Nonetheless, for consistency with previous studies, we use the term NCP_{POC} to describe the quantities computed in Eq. 8.

$$NCP_{POC,D\ or\ N} = z_{mld} \left.\frac{dPOC}{dt}\right|_{D\ or\ N} + F_{mix(POC)} \quad (8)$$

$$GPP_{POC} = \frac{t_d(NCP_{POC,D} - NCP_{POC,N})}{PQ} \quad (9a)$$

$$CR_{POC} = \frac{NCP_{POC,N}}{PQ} \quad (9b)$$

$$NCP_{POC,24hr} = \frac{t_d NCP_{POC,D} + t_N NCP_{POC,N}}{(t_d + t_N)} \quad (9c)$$

The presence of significant upwelling at drifter site 1 provides additional complexity in the estimate of NCP from optically-derived POC measurements. In particular, vertical transport of particle-poor seawater from below the mixed layer into the surface could dilute the c_p signal used

to derive POC concentrations (Stramska and Dickey, 1994). To address this, we applied the vertical mixing term, k_{mix}, derived from Eq. (6) to estimate the average daily dilution effect on mixed layer POC concentrations through drifter period 1:

$$F_{mix,POC} = k_{mix} \frac{dPOC}{dz} \quad (10)$$

The term d[POC]/dz represents the vertical gradient in [POC], derived from daily average POC concentrations measured in Rosette samples at 5 m and near the base of the euphotic zone, below the mixed layer (40–60 m) (Sect. 2.4). The dz term was calculated as the difference between the average mixed layer depth from all CTD casts and the daily average shallowest depth of minimum particle concentrations based on beam transmission profiles. The uncertainty associated with this gradient calculation is addressed in the discussion section. At drifter site 2, $F_{mix,POC}$ was considered negligible (Sect. 2.6.1) due to the high density stratification of the water column.

In total, three sets of 24-hour GPP, CR and NCP values were calculated during the drifter 1 deployment from the three pairs of consecutive day and night intervals, starting with the first night interval and ending with the last day interval. We excluded the first day-time interval from our calculations, due to the erratic salinity values observed during the first day of this drifter deployment (Sect. 3.1; Fig. S3). Because the drifter period was terminated prior to sunset, the last day interval was 1.6 hours shorter than the average daytime duration. For the second drifter deployment, two sets of GPP, R and NCP values were calculated from consecutive day and night intervals, starting with the first daytime interval and ending with the last nighttime interval. The initiation of the drifter period occurred after sunrise, so the first day interval was 1.1 hours shorter than the average daytime duration.

2.6.3 Integration time scales

The approach to calculating NCP on the basis of linear regressions utilizes the high temporal resolution of our data set. We compared our results from Sects. 2.6.1 and 2.6.2 to NCP values calculated using several of other integration time scales. Following studies that have calculated daily NCP values from "instantaneous" rates of change (e.g., hourly rates in Hamme

et al., 2012; Tortell et al., 2014), we divided our NCP calculations into shorter increments. Given that the average measurement interval was ~15 minutes (after removing values where the ship was not sufficiently close to the drifter; Sect. 2.1), we calculated NCP within three-hour intervals:

$$NCP_{\frac{O2}{Ar},3hr} = \frac{3}{24}\left[z_{mld}\left(\frac{dO_{2bio}}{dt}\right)_{3hr} + J_{ex,3hr}\right] \quad (11a)$$

$$NCP_{POC,3hr} = z_{mld}\left[\frac{3}{24}\left(\frac{dPOC}{dt}\right)_{3hr}\right] \quad (11b)$$

For each day of the drifter periods, eight consecutive three-hour NCP values were summed into a 24-hour period to yield daily NCP estimates. We then applied the vertical mixing correction to these daily estimates (refer to Eqs. 5, 6, 10), since the correction was only available on a daily basis given the lower sampling resolution of [N_2O] and [POC] profiles. We also calculated daily NCP using the difference between $\Delta O_2/Ar$ or [POC] between two time points at the beginning and end of each 24-hour period (similar to approach in Alkire et al. 2012; and Barnes and Antoine, 2104). Finally, we calculated a single daily NCP rate per drifter period using the linear regression of $\Delta O_2/Ar$ and [POC] against time over the entire drifter period. For these latter two approaches, the 24-hour average and drifter-period average of relevant terms in Eqs. 1-9 were used to calculate NCP, respectively.

2.7 Error analysis

Errors for all estimates of net primary productivity (CbPM-NPP, ^{14}C-NPP) and net community production ($NCP_{O2/Ar}$, NCP_{POC}) were propagated from uncertainties associated with all variables used for the computations. Error estimates for time-averaged variables were generally represented by the standard deviation, as we assumed that this significantly exceeded the error of the individual variables prior to averaging. The uncertainty in z_{mld}, derived from the standard deviation of mixed layer depths across individual CTD casts, was 2 m for drifter site 1 and 5 m for drifter site 2 (Sect. 2.3). Small uncertainties in t_D and t_N were calculated as the standard deviations of all day or night lengths measured during both drifter periods (0.14 and 0.10 hours, respectively). Mean relative errors of [Chl-a] and [C_{ph}] from Burt et al. (2018), and

mean relative standard deviations in MODIS-derived daily surface PAR values were propagated to calculate the error in CbPM-NPP. The standard deviations of triplicate 24-hour ^{14}C uptake incubations were propagated to calculate the error in ^{14}C-NPP estimates. The uncertainties in ^{14}C-NPP values are likely underestimated, as they do not account for bottle effects, as discussed in Sect. 4.3.

For calculating error in NCP, uncertainties in dO_{2bio}/dt and dPOC/dt were derived from the confidence interval of the best-fit slope of linear regression of each variable against time. Standard deviations of averaged $\Delta O_2/Ar$, k_{O2}, and k_{N2O} values, and the mean relative errors of $[N_2O]_{meas}$, $[N_2O]_{Eq}$, $[N_2O]_{thermal}$, and $\frac{dO_{2bio}}{dN2O_{bio}}$ reported in Izett et al. (2018), were propagated into the mixing correction errors for $NCP_{O2/Ar}$ and NCP_{POC}. The error in $\frac{dN2O_{bio}}{dz}$ was calculated as the confidence interval of the best fit slope extracted from a linear regression of pooled drifter 1 $[N_2O]_{bio}$ values against depth. Finally, to account for uncertainty in the photosynthetic quotient (PQ), we applied a PQ variability of 0.1 to $NCP_{O2/Ar}$ calculations, following Laws (1991).

3 Results

3.1 Water mass properties

Ship-board underway measurements revealed clear differences in hydrographic and biogeochemical characteristics between the water masses sampled by the two drifters. Surface water properties at drifter site 1 reflected the presence of a recently upwelled water mass that was relatively cold (11.8 ± 0.4 °C), saline (32.6 ± 0.04 g/kg), and nutrient-rich (Figs. 1, S3, S4). The Pacific Fisheries Environmental Laboratory's coastal upwelling index at 45°N, 125°W was positive throughout drifter period 1. In contrast, the water mass tracked by the second drifter deployment was warmer (17.5 ± 0.1°C) and fresher (31.8 ± 0.05 g/kg), with lower average mixed layer nutrient concentrations.

Examination of surface water hydrographic properties during the two drifter deployments suggest that both drifters tracked a relatively homogenous water mass, excluding a period of salinity variability during the first day of drifter deployment 1, and several transient temperature and salinity excursions after the second night of this deployment (grey patches in Fig. S3). These

features indicate potential intrusion of an external water mass, possibly a result of loss of the drifter drogue (Sect. 2.1). Observations during these periods were thus removed from the data set prior to analysis to ensure the most accurate calculation of productivity rates. Outside of these intervals, variability in salinity (drifter 1: 32.5–32.7 g/kg; drifter 2: 31.8–31.9 g/kg) was small during both drifter deployments. Variability in sea surface temperature was also limited (drifter 1: 11.2–13.0 °C, drifter 2: 17.3–17.7 °C), and largely reflected a diurnal variation of warming and cooling, which was particularly evident for drifter period 2.

Temporal differences in CTD cast profiles point to some variation in mixed layer depth (z_{mld}) during both drifter deployments. In general, there were no multi-day trends or regular diurnal patterns in z_{mld} through both periods, suggesting that transient shifts in water column turbulence likely contributed to changes in the shape of temperature, salinity, dissolved oxygen and fluorescence profiles. Average z_{mld} values, calculated over each drifter period, had relatively low relative standard deviations (<25%) and were applied to all subsequent calculations (Sect. 2.3). A sensitivity analysis, not shown, indicated that the choice of mixed layer depth using different criteria (i.e., fluorescence profiles, density profiles and the density difference criterion) and different time scales of integration (i.e., daytime/nighttime, 24 hour, and multi-day) did not significantly impact the results discussed below.

Average mixed layer nutrient concentrations fluctuated during both drifter deployments, but did not exhibit regular diurnal cycles (Fig. S4). At drifter site 1, concentrations ranged from 0.74 to 0.85 µM phosphate, 7.8 to 9.0 µM nitrate and nitrite, and 9.2 to 11.1 µM dissolved silica, excluding day 1 of the drifter deployment and anomalously high concentrations measured during a noisy CTD cast at midnight on the last day of the deployment. Excluding these outliers, a significant ($p<0.05$) linear regression of each nutrient concentration against time revealed that phosphate concentrations decreased by ~0.07 µM, [NO_3^- + NO_2^-] decreased by 0.9 µM, and [SiO_2] decreased by 1.2 µM over the three-day drifter period, roughly in Redfield ratio proportions (Sect. 3.4). Nutrient concentrations varied less at site 2, from 0.08–0.10 µM [PO_4^{3-}], 0.29–0.61 µM [NO_3^- + NO_2^-], and 1.2–1.7 [SiO_2]. While [PO_4^{3-}] and [SiO_2] increased significantly ($p<0.05$) by 0.015 µM and 0.48 µM, respectively, these changes were small compared to the shift observed during drifter period 1, and did not reflect Redfield ratio proportions. It is possible that intrusions of an external water mass with slightly elevated nutrient concentrations have contributed to the small increase in [PO_4^{3-}] and [SiO_2] measured during

these CTD casts, even though we assume that such effects on our derived productivity estimates are negligible based on inspection of underway temperature and salinity data (Fig. S3).

3.2 Biogeochemical comparisons between drifter sites

Elevated nutrient concentrations at the drifter 1 site supported high productivity and the accumulation of phytoplankton biomass, as indicated by elevated chlorophyll-a ([Chl-a]= 0.66–1.5 µg/L), phytoplankton carbon ([C_{ph}]= 83–115 µg/L) and particulate organic carbon concentrations ([POC]= 130–261 µg/L) (Figs. 2a–c). We observed [C_{ph}]/[Chl-a] ratios ranging from 68–143 g/g, with a median value of 85 g/g (Fig. 2f). Using the carbon-based production model (CbPM; Sect. 2.5) and daily-averaged mixed layer PAR derived from satellite values matched to drifter location (within 5 km), these [C_{ph}]/[Chl-a] ratios translate into phytoplankton growth rates ranging from 0.75–0.94 d^{-1}. At the second drifter site, phytoplankton productivity and biomass were significantly lower in the nutrient-poor waters ([Chl-a]= 0.06–0.21 µg/L, [C_{ph}]= 11–17 µg/L, and [POC]= 25–38 µg/L). Ratios of [C_{ph}] to [Chl-a] at site 2 were significantly higher ($p<0.05$) than those observed at site 1, ranging from 69 g/g to 203 g/g, with a median value of 108 g/g. The higher ratios may reflect reduced cellular [Chl-a] associated with greater nutrient limitation, higher daily-integrated PAR, and proportionally more picoplankton than microplankton at drifter site 2 (Westberry et al., 2008; Hirata et al., 2011; Graff et al., 2016; Burt et al., 2018). Median PAR levels were higher and less variable at site 2, in part contributing to lower variability in CbPM-based growth rates, which ranged from 0.81 to 0.85 d^{-1}.

Several lines of evidence suggest that the phytoplankton assemblage at drifter site 1 was enriched in large-celled phytoplankton, as compared to drifter site 2. The wavelength-dependent slope of particulate backscatter (b_{bp}) was lower at site 1 (range: 1.4 to 1.6, median: 1.5) than at site 2 (range: 1.9–2.3, median: 2.1) (Fig. 2d), suggesting proportionally larger particle sizes (Stramska et al., 2003; Kostadinov et al., 2009). This observation is supported by size-fractionated Chl-a measurements. During the drifter 1 deployment, the >20 µm size fraction (Sect. 2.4), increased from 21 % to 46 % of the total Chl-a pool, indicating the enrichment of large phytoplankton in the assemblage. Indeed, pigment-based estimates of phytoplankton taxonomic composition and size class (Hirata et al., 2011; Zeng et al., 2018) suggested that relative diatom and microplankton abundances exceeded 50% on the final sampling time point.

By comparison, size-fractionated [Chl-a] and HPLC analyses from drifter 2 indicated a lower proportion of large-celled phytoplankton, with 9–15% of total Chl in the >20 μm size fraction, and diatoms and micro-plankton comprising 19–29% of the phytoplankton assemblage. The proportion of picoplankton increased through time at drifter site 2 from 31–50% of total [Chl-a], alongside slight increase in b_{bp} slope, indicating accumulation of smaller particle sizes (Fig. S3d). Finally, median bulk refractive index values across three wavelengths (470 nm, 532 nm, 650 nm) were higher at site 1 (1.08–1.11) than at site 2 (1.02–1.04) (Fig. S3e), which is consistent with a greater proportion of diatom-derived amorphous silica in the particle pool (Lide, 1997; Twardowski et al., 2001).

3.3 Diurnal variability and primary production

As shown in Fig. 3a, clear diurnal cycles in biological oxygen saturation ($\Delta O_2/Ar$) were observed during both drifter deployments. Generally, values of $\Delta O_2/Ar$ increased from dawn to dusk and decreased from dusk to dawn, yielding positive slopes of linear regressions of $\Delta O_2/Ar$ against time in the daytime, and negative slopes at night (Fig. S5a). During drifter deployment 1, this diurnal cycle was superimposed on a longer-term increase in biological O_2 saturation as under-saturated values returned toward atmospheric equilibrium. At least part of this increase is attributable to gas exchange, which would act to erase O_2 under-saturation in the mixed layer caused by recent upwelling. However, calculation of the sea-air O_2 flux shows that, except for the first 24-hour period, only a small amount of the daily increase in $\Delta O_2/Ar$ can be explained by gas exchange (absolute value of J_{ex} < 10 mmol O_2 m^{-2} d^{-1}) (Table 1). Thus, the temporal change in $\Delta O_2/Ar$ can be attributed to a primarily biological source. The magnitude of this increase is further underestimated because of vertical upwelling of deep oxygen-poor waters, which would act to dampen the increase in $\Delta O_2/Ar$ through time. After accounting for a mixing correction ranging between 22 and 97 mmol m^{-2} d^{-1} O_2 (equivalent to 16 to 70 mmol m^{-2} d^{-1} C when assuming a photosynthetic quotient of 1.4), daily-integrated gross primary productivity ($GPP_{O2/Ar}$) ranged from 270 to 358 mmol C m^{-2} d^{-1}, and community respiration ($CR_{O2/Ar}$) rates ranged from 74 to 172 mmol C m^{-2} d^{-1} (Table 1).

Examination of the diel variability in POC and Chl-a during drifter period 1 revealed significant differences in the behavior of these variables as compared to $\Delta O_2/Ar$ (Fig. 3b, c).

Namely, $\Delta O_2/Ar$ increased during the first drifter deployment, whereas [POC] and [Chl-a] values decreased. We estimated that vertical mixing ($F_{mix,POC}$), accounted for 12 to 68 mmol m^{-2} d^{-1} C of these daily changes in [POC], similar to the magnitude of the mixing correction for $\Delta O_2/Ar$ variability (Table 1). After taking mixing into account, daily-integrated GPP_{POC} decreased from 242 mmol m^{-2} d^{-1} on day 1 to 98 mmol m^{-2} d^{-1} on day 3, while CR_{POC} rates ranged from 77 to 147 mmol m^{-2} d^{-1}.

Calculated daily averaged net primary productivity (NPP) were lower than $GPP_{O2/Ar}$. Rates derived from the CbPM model (Sect. 2.5), declined from 147 mmol C m^{-2} d^{-1} on day 1 of drifter deployment 1 to 112 mmol C m^{-2} d^{-1} on day 3 (Table 1), reflecting the trend in Chl-a concentrations used to derive NPP (Fig. 3c). The CbPM-derived NPP estimate was similar to that obtained in ^{14}C incubations (150 ± 18 mmol C-$m^{-2}d^{-1}$) within the first 24 hours of drifter deployment 1. However, ^{14}C-based NPP estimates on the third day of the deployment (49 ± 8 mmol C-$m^{-2}d^{-1}$) were about two-fold lower than those obtained from CbPM calculations.

Dissolved oxygen and POC dynamics at drifter site 2 differed significantly from those observed at site 1. Compared to the drifter site 1, diel variability in $\Delta O_2/Ar$ and [POC] was more tightly coupled during the second drifter deployment (Fig. 3a, b). Both O_2/Ar and [POC] displayed regular diurnal variations, increasing in the daytime to a maximum around dusk and decreasing at night to a minimum around dawn (Fig. S5a, b). Over the full drifter deployment, concentrations of Chl-a and, to a lesser extent, POC, decreased, in contrast to $\Delta O_2/Ar$, which remained relatively constant across days. Daily-integrated $GPP_{O2/Ar}$ values ranged from 108 to 219 mmol C m^{-2} d^{-1} and $CR_{O2/Ar}$ rates ranged from 82 to 186 m^{-2} d^{-1}. POC-derived values were considerably lower and less variable, from 41 to 38 for GPP_{POC} and 36 to 44 for CR_{POC} (Table 1). NPP derived from CbPM calculations was 22 mmol C m^{-2} d^{-1} on the first day of the drifter period and 18 mmol C m^{-2} d^{-1} on the second day, while NPP calculated from one ^{14}C bottle incubation during the first day of the drifter 2 deployment was 12 ± 4 mmol C m^{-2} d^{-1}, showing good agreement with the CbPM calculations.

3.4 Net community production

Daily net community production (NCP) rates were calculated using linear regressions of $\Delta O_2/Ar$ and POC over day and night intervals, corrected for gas exchange and vertical mixing

(Sect. 2.6.1, 2.6.2). During drifter period 1, $NCP_{O2/Ar}$ and NCP_{POC} exhibited contrasting trends, as $NCP_{O2/Ar}$ remained >100 mmol C m^{-2} d^{-1} throughout, while NCP_{POC} declined to negative values on the second and third days (Table 1; Fig. 4). At drifter period 2, we observed closer agreement between NCP values. $\Delta O_2/Ar$-derived NCP ranged from -12 to 33 mmol C m^{-2} d^{-1} over two consecutive 24 hour periods, while NCP_{POC} values ranged from -3 to 1 mmol C m^{-2} d^{-1}. These lower rates at drifter site 2 are consistent with the lower observed phytoplankton biomass and nutrient concentrations.

Additional constraints on NCP during drifter period 1 can be derived from examining nutrient drawdown. Because vertical upwelling of nutrient-replete waters would dampen the magnitude of observed nutrient drawdown over time (Sect. 3.1), we used the derived k_{mix} from Eq. 6 and a best-fit vertical gradient in nutrient concentrations between the mixed layer and 100 m (Sect. 2.4) to account for this mixing flux. This correction increases the cumulative three-day nutrient drawdown by 2.1 to 2.6 times. Over the three-day drifter deployment (Sect. 3.1), surface Si, N and P concentrations declined in a ratio of 17: 13: 1, which is consistent with the stoichiometry expected for organic matter produced by a diatom-rich assemblage (Brzezinski et al., 1998; Turner et al., 1998; Brzezinski, 2004). Assuming that the observed decrease in SiO_2 concentrations over the three days is attributable to growth of diatoms in the mixed layer, and applying a stoichiometric ratio of 106 C: 16 Si, we estimate an average C fixation rate of ~128 mmol C m^{-2} d^{-1} for the drifter period. This value is consistent with $NCP_{O2/Ar}$ rates, which were 137 mmol C m^{-2} d^{-1} on average over three days, but significantly greater than NCP_{POC} estimates (7 mmol C m^{-2} d^{-1} on average) (Table 2).

Table 2 summarizes comparisons among NCP values calculated using day/night linear regressions of $\Delta O_2/Ar$ and POC against time, and other approaches described in Sect. 2.6.3. In general, our main conclusions were not significantly altered by different calculation methods. NCP values derived from one linear regression over each drifter period agreed well with the average of two (drifter 2) to three (drifter 1) daily NCP values calculated via the other approaches. Small differences between linear regression-based NCP values and both NCP calculated from either 3-hour increments or two time points are likely due to the effect of lower signal to noise in $\Delta O_2/Ar$, $[O_2]_{bio}$ and [POC] values utilized in these latter two approaches. Thus, the following discussion focuses on productivity rates derived from day/night linear regressions (i.e., Eqs. 1 and 8) because they utilize all data points while minimizing uncertainty in the

derived rates of change. The exception is the $NCP_{O2/Ar}$ value calculated for day 1 of drifter period 2 using the daytime/nighttime linear regression method. By this approach, we calculated $NCP_{O2/Ar}$ as 26 mmol C m^{-2} d^{-1}, even though the time series in Fig. 3a clearly indicates a net decrease in $\Delta O_2/Ar$ over the 24-hour period, and all other $\Delta O_2/Ar$-based NCP calculations (Sect. 2.6.3) yielded negative values. For the discussion, Table 1 and Fig. 4, the NCP value derived from the integrated 3-hour increments represents net community production during this particular interval.

4 Discussion

The results from our Lagrangian surveys illustrate diurnal dynamics in two contrasting productivity regimes off the Oregon coast. Biogeochemical properties during the first drifter deployment suggested a dynamic, highly productive phytoplankton community, influenced by upwelling and elevated mixed layer nutrient concentrations (Figs. 1, S4). Several lines of evidence imply the presence of a developing diatom bloom at this site (Sect. 3.2; Figs. 2, 3). Increasing mixed layer biological oxygen saturation ($\Delta O_2/Ar$) was contrasted by a general decrease in particulate organic carbon (POC) concentrations, suggesting a significant decoupling between O_2 and POC dynamics. This was reflected in significant differences between $\Delta O_2/Ar$-derived gross primary productivity (GPP) and net community production (NCP) rates derived from $\Delta O_2/Ar$ and POC measurements (Figs. 4, 5; Table 1). In contrast, biogeochemical properties during the second drifter deployment were indicative of a lower productivity, nutrient-limited phytoplankton assemblage, with near-zero $\Delta O_2/Ar$ values reflecting a close balance between water column photosynthesis and respiration (Fig. 3a). Relative to the drifter 1 site, diurnal variations in $\Delta O_2/Ar$ and POC were more closely coupled, while phytoplankton biomass (C_{ph}) and chlorophyll-a (Chl-a) concentrations (dominated by smaller cells) varied little through time. Contrary to our expectations, even though $NCP_{O2/Ar}$ and NCP_{POC} rates agreed well, we also observed significant discrepancies between $GPP_{O2/Ar}$ and GPP_{POC}, and different community respiration rates ($CR_{O2/Ar}$ and CR_{POC}) during drifter period 2. The contrasting properties between the two drifter deployments enable us to examine the coupling of O_2 and POC dynamics under different ecological states, with implications for the use of $\Delta O_2/Ar$ and POC measurements as proxies for GPP and NCP.

655

656 **4.1 Decoupling of O_2 and POC dynamics in the mixed layer**

657

658 **4.1.1. Drifter 1.** In the absence of significant POC sinking and net loss to the dissolved
659 organic carbon (DOC) pool, POC-based productivity rates should approximate O_2/Ar-based rates
660 (Claustre et al., 2008; White et al., 2017). However, at drifter station 1, both $GPP_{O2/Ar}$ and
661 $NCP_{O2/Ar}$ greatly exceeded GPP_{POC} and NCP_{POC}, respectively (Figs. 4, 5a; Table 1). Over the
662 three successive 24-hour periods of drifter deployment 1, the absolute difference between GPP
663 measures increased from 41 mmol C m^{-2} d^{-1} to 260 mmol C m^{-2} d^{-1}, while the absolute difference
664 between NCP estimates increased from 42 mmol C m^{-2} d^{-1} to 193 mmol C m^{-2} d^{-1}. The NCP
665 differences exceeded the propagated uncertainties in NCP during second and third days of the
666 deployment. The transition to negative NCP_{POC} values over the course of the drifter 1
667 deployment primarily reflected diminishing daytime rates of POC accumulation (dPOC/dt term
668 in Eq. 8) (Fig. S5).

669 This apparent discrepancy between $NCP_{O2/Ar}$ and NCP_{POC} is consistent regardless of the
670 approach used to calculate NCP rates (Sect. 2.6.3, Table 2). However, comparisons of ΔO_2/Ar-
671 derived NCP relative to POC-derived NCP in 3-hour increments (Eq. 11) can reveal
672 discrepancies on shorter time scales than daily-integrated values (Fig. 5c). Taken together, these
673 GPP and NCP comparisons suggest that additional POC losses decoupled O_2 from POC
674 dynamics during drifter period 1. While mixed layer ΔO_2/Ar was primarily impacted by the
675 accumulation of O_2 from gross primary production (GPP) and O_2 loss from community
676 respiration, diurnal variability in [POC] was likely affected by several additional loss factors,
677 including particle export, photooxidation, grazing, and DOC production.

678 During a diatom bloom, enhanced aggregation of large silica-rich particles and
679 zooplankton fecal pellet production can stimulate export of POC and diatom cells out of the
680 mixed layer, progressively decreasing NCP_{POC} relative to $NCP_{O2/Ar}$. A number of previous
681 studies have reported enhanced particle fluxes associated with diatom blooms in various oceanic
682 regions (Buesseler, 1998; Guidi et al., 2009; Brzezinski et al., 2015; Stukel et al., 2017) . The
683 global compilation of Henson et al. (2012) reported maximum export fluxes of ~83 mmol C m^{-2}
684 d^{-1} from Southern Ocean measurements, while Alkire et al. (2012) derived maximum export
685 fluxes of 96 mmol C m^{-2} d^{-1} during termination of the North Atlantic spring bloom. Stukel et al.

(2017) applied the steady-state ^{234}Th-^{238}U approach to quantify export fluxes of ~36 mmol C m^{-2} d^{-1} in the nearshore region of the Southern California Current system. The higher value estimates are in the range of the discrepancy we observed between NCP_{POC} and $NCP_{O2/Ar}$, suggesting that POC export fluxes could potentially account for a significant fraction of the inferred POC loss at drifter site 1.

Another likely POC loss is DOC production through cellular exudation, viral lysis and/or grazing (Briggs et al., 2018; Claustre et al., 2008; Dall'Olmo et al., 2011; Lochte et al., 1993). Loss of POC to the DOC pool would lower NCP_{POC} without affecting $NCP_{O2/Ar}$ values if the DOC produced is not respired in the mixed layer. While we did not conduct direct measurements of DOC concentrations during the cruise, previous work in a variety of ocean environments has shown that DOC production can account for 3-37% of NCP in the Ross Sea, up to 10-40% in the equatorial Pacific Ocean, and up to 66% in the Sargasso Sea during the seasonal phytoplankton bloom (Hansell and Carlson, 1998). More recently, Alkire et al. (2012) estimated that 22-40% of NCP was released into the DOC pool during the North Atlantic bloom, and Bif and Hansell (2019) estimated springtime ΔDOC/NCP ratios of 0.05 – 0.54 and summertime ratios of 0 – 0.28 along the Line P transect (130 – 152 °W) in the eastern Subarctic Pacific. In the results of Bif and Hansell (2019), the most comparable Line P measurement to drifter station 1 (in terms of location and [Chl-a]) exhibited a ΔDOC/NCP ratio of 0.19 in the summer and 0.34 in the spring, implying that up to 34% of NCP was partitioned into the DOC pool. Assuming a lower bound of ~20% of NCP released as DOC yields a daily-integrated DOC flux of 21 to 33 mmol C m^{-2} d^{-1}. The remaining discrepancy between ΔO_2/Ar and POC-based NCP estimates (14 to 159 mmol C m^{-2} d^{-1}; average, 103 mmol C m^{-2} d^{-1}) is potentially attributable to particle export. Taking an upper bound of 40% of NCP as DOC production, which is closer to the easternmost station sampled in Bif and Hansell (2019), yields a daily-integrated DOC flux of 56 to 67 mmol C m^{-2} d^{-1} (Fig. 4) and a residual export flux of -14 to 126 mmol C m^{-2} d^{-1} (average, 76 mmol C m^{-2} d^{-1}) (Table 1). This range of results demonstrate that DOC production cannot likely account for the full discrepancy between ΔO_2/Ar and POC-based NCP estimates at drifter site 1, suggesting that export fluxes are likely a significant mechanism for mixed layer POC loss.

A final consideration involves diurnal variation of zooplankton abundances and grazing rates, which may introduce an additional POC loss process that contributes to decoupling between mixed layer POC/C_{ph} and dissolved ΔO_2 dynamics (Dall'Olmo et al., 2011; Briggs et

al., 2018). During our expedition, we observed a strong signature of diel migrating zooplankton based on increased night-time signal spikes in surface optical backscatter measurements (Burt and Tortell, 2018). In addition to particle sinking and DOC excretion, these nighttime migrations could enhance POC and C_{ph} loss at night without depleting $\Delta O_2/Ar$, if POC uptake rates exceed respiration rates. For example, (Wu et al., 2010) observed that mesozooplankton prefer to graze diatom-dominated assemblages at night over day in the East China Sea. Assuming that biomass accumulation rates from grazing surpasses grazer respiration rates (Dagg et al., 1982), these diurnal variations would contribute to more POC loss than O_2 loss. In addition, once POC is assimilated into the body of a grazer, it joins a larger particle size class that likely exceeds the size-dependent detection limits of the beam attenuation coefficient (Stramski and Kiefer, 1991; Marra, 2002; Claustre et al., 2008;), decreasing the c_p signal used to derive POC.

4.1.2 Sub-daily variations in community respiration. Although $GPP_{O2/Ar}$ generally exceeded GPP_{POC} during drifter period 1, differences in $CR_{O2/Ar}$ and CR_{POC} were smaller and not statistically significant throughout the drifter period (Fig. 5b). During days two to three, the $CR_{O2/Ar}$ values were larger than CR_{POC} values. Thus, the discrepancies between $NCP_{O2/Ar}$ and NCP_{POC} (Sect. 4.1.1) may be attributed more to differences in gross accumulation of POC and O_2 (Claustre et al., 2008; White et al., 2017), rather than to differences in POC and O_2 losses. This suggests that POC loss rates varied on sub-daily time scales through drifter deployment 1, and were generally higher in the daytime than at night. This is supported by a weak correlation between $\Delta O_2/Ar$-based and POC-based 3-hour NCP ($p<0.05$, $r_2= 0.39$) in Fig. 5c, which suggests that the magnitude of decoupling between $\Delta O_2/Ar$ and POC dynamics varies throughout the day. Indeed, the increasing discrepancy between $NCP_{O2/Ar}$ and NCP_{POC} between days 1 and 3 of the drifter period suggests increasing POC loss rates over this time frame.

In the dynamic, high productivity upwelling environment of drifter site 1, a number of day/night variations in grazing rates, export fluxes, particle sinking velocities, DOC production rates and mixed layer properties could lead to greater differences between $GPP_{O2/Ar}$ and GPP_{POC} than between $CR_{O2/Ar}$ and CR_{POC} (Waite and Nodder, 2001; Gernez et al., 2011; White et al., 2017; Briggs et al., 2018). Lower nighttime grazing relative to daytime rates would diminish CR_{POC} relative to $CR_{O2/Ar}$ (White et al., 2017; Briggs et al., 2018). However, grazing is typically more pronounced at night due to upward vertical migration of zooplankton (e.g., Burt and

Tortell, 2018). Mixed layer depth changes, particularly shoaling in the day and deepening at night, can enhance POC export fluxes in the day and lower fluxes at night (Gardner et al., 1999; Briggs et al., 2018). However, we did not observe any consistent diel patterns in mixed layer depth at drifter station 1.

More likely, higher DOC production relative to DOC respiration in the day and vice-versa at night would cause $GPP_{O2/Ar}$ to increase more than GPP_{POC} in the daytime, while causing $CR_{O2/Ar}$ to exceed CR_{POC} rates in the nighttime. Such light-dependent increases in DOC production, could result, for example, from the effects of photo-respiration and other mechanisms of dissipating excess light energy. Indeed, we observed evidence of photo-oxidative stress during the daytime from increased non-photochemical quenching activity in phytoplankton assemblages (Schuback et al., 2019). Finally, growth in cell size during the day could lead to higher daytime export rates, while also causing proportionally more particles to escape detection by the ac-s sensor in the daytime relative to at night, when increased cell division and depression of particle sizes could increase the number of particles detected by the ac-s sensor (DuRand and Olson 1996; Oubelkheir and Sciandra, 2008; Khierrediene and Antoine, 2014). We did not find consistent changes in cell size from the particulate backscatter time series or *in situ* measurements of size-fractionated [Chl-a] between day and night. Nonetheless, without direct measurements of particle size, export fluxes, or DOC production, we cannot rule out the influence of diurnal variations in such rates on our productivity estimates.

Taken together, the potential variations in POC loss rates on sub-daily time scales suggest that comparing only GPP or only CR estimates based on nighttime linear regressions of $\Delta O_2/Ar$ and POC against time (Eqs. 1, 8) could yield erroneous estimates of POC loss. By comparison, differences in daily $NCP_{O2/Ar}$ and NCP_{POC} provide a more robust indicator of cumulative POC loss, as illustrated by the relatively consistent discrepancies between all calculated $NCP_{O2/Ar}$ and NCP_{POC} values in Table 2.

4.1.3 Drifter 2. Drifter site 2 exhibited comparable absolute discrepancies between $GPP_{O2/Ar}$ and GPP_{POC} and greater discrepancies between $CR_{O2/Ar}$ and CR_{POC} relative to drifter site 1 (Fig. 5a-b; Table 1). A scatterplot of $\Delta O_2/Ar$-derived NCP and net [POC] change in 3-hour increments (Eq. 11) shows that the magnitude of $\Delta O_2/Ar$-derived changes consistently exceeds the magnitude of POC-derived changes throughout the drifter period, no matter the time of day

779 (Fig. 5d). The strong, positive relationship between these two 3-hour measures ($p<0.05$, $r_2=0.64$),
780 compared to the weaker correlation at drifter site 1 (Fig. 5c), suggests that despite large
781 differences in the magnitude of $\Delta O_2/Ar$-derived and POC-derived GPP and CR rates, POC-based
782 changes are a good relative indicator of O_2-derived productivity rates.
783 Prior studies have observed that the amplitude of diurnal variability in $\Delta O_2/Ar$ exceeds
784 the amplitude of diurnal variability in c_p-based [POC]. For example, in their North Atlantic
785 bloom survey, Briggs et al. (2018) observed higher amplitude variations in O_2 relative to c_p-
786 derived [POC], leading to higher absolute O_2-derived respiration and gross oxygen production
787 (GOP) rates compared to c_p-derived rates throughout stages of the bloom. A photosynthetic
788 quotient (PQ) of 1.45 (from Laws 1991) was not sufficient to reconcile GOP with GPP_{cp}. In the
789 Southern Ocean, Hamme et al. (2012) also observed high ratios of underway $\Delta O_2/Ar$-derived
790 gross oxygen production to gross carbon production (i.e., GPP) based on photosynthesis-
791 irradiance incubations, surpassing the expected range for the photosynthetic quotient. At a
792 relatively low productivity site with low phytoplankton biomass (Table 1; Fig. 2), heterotrophic
793 bacteria can comprise a substantial fraction of total living biomass in the mixed layer, and
794 variations in their total biomass can impact c_p measurements (Oubelkheir and Sciandra, 2008;
795 Barnes and Antoine, 2014). If detected by the ac-s sensor, bacteria could potentially account for
796 some of the discrepancy between diel POC and O_2-derived variability at drifter site 2. Assuming
797 that DOC exudation from phytoplankton cells is positively related to growth in heterotrophic
798 biomass, either from direct DOC consumption, or indirectly through external drivers such as
799 irradiance levels (Kuipers et al., 2000; Fuhrman et al., 1985; Church et al., 2004; Oubelkheir and
800 Sciandra, 2008), c_p decreases from phytoplankton exudation would counter c_p increases from
801 heterotrophic growth. At night, this would decrease CR_{POC} rates derived from c_p-based [POC],
802 relative to O_2-derived CR rates. Indeed, the positive $CR_{O2/Ar}$ - CR_{POC} discrepancy contributed to
803 58-82% of the differences between $\Delta O_2/Ar$ and POC-derived GPP rates at drifter station 2. The
804 remaining difference may be attributed to POC losses to the DOC pool or other sinks (discussed
805 below) in the daytime.
806 Because daytime increases in both $\Delta O_2/Ar$ and [POC] are balanced by respective
807 nighttime decreases, absolute differences in $NCP_{O2/Ar}$ and NCP_{POC} were smaller than at drifter
808 site 1. While, this discrepancy was negligible over the first 24-hour period, it increased to 32
809 mmol C $m^{-2}d^{-1}$ over the 24-hour period (Table 1; Fig. 4), exceeding the uncertainty of both NCP

calculations. Overall, the closer absolute agreement across NCP estimates is consistent with the view of drifter site 2 as a more oligotrophic ecosystem, where primary production and heterotrophic consumption are more tightly coupled (Claustre et al., 2008; White et al., 2017). The smaller absolute differences between $NCP_{O2/Ar}$ and NCP_{POC} suggest a lower, but non-negligible, potential for POC sinking, grazing and net DOC production over consumption to decouple POC, C_{ph} and $\Delta O_2/Ar$ dynamics at drifter site 2. Although we lack direct DOC measurements, lower 440 nm absorption values in the filtration blanks (Sect. 2.2) at drifter site 2 compared to drifter site 1 suggest lower colored dissolved organic matter (CDOM) concentrations (Organelli et al., 2014; Peacock et al., 2014). This observation is consistent with several previous observations of lower net DOC production in lower productivity and/or oligotrophic waters (Bif et al., 2018; Hansell and Carlson, 1998). A recent compilation of summertime DOC production and NCP measurements along the Line P transect in the Northeast Pacific Ocean, shows that DOC production comprises at most 28% of total NCP in offshore waters (Bif and Hansell, 2019). Even DOC/NCP ratios as high as 28% at drifter site 2 would result in low overall DOC accumulation, because NCP rates were relatively low.

Low particle sinking rates are another factor that can explain the smaller absolute discrepancy between $NCP_{O2/Ar}$ and NCP_{POC} at drifter site 2. Low particle export is generally expected from phytoplankton assemblages dominated by small particle sizes <20µm, consistent with the higher b_{bp} slope values and Chl-a size fractionation measurements at drifter site 2 (Sect. 3.2; Fig. 2) (Fowler and Knauer, 1986; Guidi et al., 2008). Nonetheless, POC export does occur under low productivity conditions, and even small export fluxes could account for the entire discrepancy between measures of NCP at drifter site 2. For example, Durkin et al., (2015) reported significant rates of particle sinking from the small-celled, oligotrophic communities that dominate the BATS station. In addition, it is possible that grazing by zooplankton would also enhance loss of these phytoplankton cells from the mixed layer (Guidi et al., 2009). As we observed at drifter site 1, increased variability in the b_{bp} signal suggest the presence of vertically migrating zooplankton into the mixed layer during nighttime intervals of drifter period 2 (Burt and Tortell, 2018). Assuming that a maximal fraction of 28% of $NCP_{O2/Ar}$ is DOC production at drifter site 2 (Bif and Hansell, 2019), a residual POC export flux of 23 mmol C m^{-2} d^{-1} would be necessary to balance $NCP_{O2/Ar}$ and NCP_{POC} during day two of the drifter period (Table 1). This

value is reasonable considering previous estimates reported from a number of lower productivity systems (Henson et al., 2012; Charette et al., 1999).

4.2 Other factors driving variability in NCP_{POC}

In interpreting our results, it is critical to consider a number of potential caveats, including methodological uncertainties and other POC sinks that could contribute to the variability in derived NCP estimates, POC export and DOC excretion rates. One important variable in all of our comparisons of productivity rates derived from biological oxygen saturation and POC is the O_2-to-POC conversion factor, represented by the photosynthetic quotient (PQ) value selected for each drifter site. Neglecting to take different respiratory quotients (RQs) into account in this O_2-to-POC conversion (e.g., Ferrón et al., 2015) may contribute to uncertainty in calculated GPP, CR and NCP rates, leading to erroneous discrepancies among derived values. But, given the relatively narrow range (~50%) of possible PQs and RQs applicable to our study sites (Laws 1991), a different PQ or RQ cannot account for the total discrepancy observed among $\Delta O_2/Ar$ and POC-derived GPP, CR and NCP rates.

In our analysis, we interpret variations in particulate backscatter (b_{bp}) and beam attenuation (c_p) in terms of phytoplankton and total particulate organic carbon concentrations, assuming a small influence of inorganic suspended minerals from the continental shelf, Columbia River discharge or other sources. However, the Columbia River plume has been observed to extend south along the coast as far as ~44.5° N in the summertime (Thomas and Weatherbee, 2006), close to the location of drifter deployment 1. Moreover, the drifter was deployed ~40 km from shore over the continental shelf, where bottom resuspension of particles and their subsequent upwelling into the mixed layer is possible. Estimates of the bulk refractive index of particles (η_p), can be used to estimate the influence of inorganic minerals in our optical measurements. During drifter deployment 1, we observed median η_p values at 470, 532 and 650 nm that were generally below 1.12 (Fig. S3e), whereas inorganic minerals in seawater, have a bulk refractive index as high as 1.26 (Lide, 1997; Twardowski et al., 2001). In addition, mixing with the fresh Columbia River plume would have significantly reduced salinity at drifter site 1 to values below 30 g/kg (Hickey et al., 1998), well below the 32 g/kg we observed during this drifter deployment (Sect. 3.1; Fig. S3c), which are consistent with salinities observed in the

offshore Northeast Pacific Ocean (Whitney and Freeland, 1999). While these relatively high salinities support our assertion of a negligible influence of riverine particles on our measurements, the observed η_p values do not preclude the presence of mixing between POC and a small fraction of shelf-derived inorganic particles at drifter site 1. By contrast, calculated η_p values during deployment 2 were below 1.08, which is close to values expected for water-containing predominantly non-diatom phytoplankton organic carbon.

Additional uncertainty in our analysis derives from the algorithms used to estimate POC and phytoplankton carbon C_{ph} from optical measurements (Sect. 2.2). Because of particle size limitations in the optical measurements, variability in seawater optical properties may not fully capture all significant components of the particulate pool, such as larger microplankton and zooplankton. Indeed, larger zooplankton often appear as erratic signal spikes in backscatter data (Burt and Tortell, 2018), which are typically filtered out during data processing. Moreover, the c_p signal at 660 nm, used to derive [POC], responds most strongly to particles within the 0.5–20 µm diameter range (Claustre et al., 2008; Marra, 2002; Stramski and Kiefer, 1991), which is smaller than many large diatoms, fecal pellets and particle aggregates. This size bias would cause an underestimate of larger particles, and therefore [POC], measured by beam attenuation, thereby contributing to the apparent discrepancy between diel changes in [POC] and diel changes in $\Delta O_2/Ar$ (Fig. 4). Despite these potential caveats, recent work (Graff et al., 2016; Briggs et al., 2018; Burt et al., 2018) has demonstrated that c_p and b_{bp}-based derivations of [POC] and [C_{ph}] can indeed be robust in high biomass ocean regions, where productivity and the proportion of large-celled phytoplankton may be greater.

Changes in the c_p-to-[POC] relationship through time could also drive apparent variability in our optical [POC] estimates during both drifter deployments. On a global scale, the linear regression of [POC] against c_p at 660 nm measured in samples from diverse marine environments is defined over a range of POC concentrations from ~5 to ~175 µg/L (Graff et al. 2015). At drifter site 2, the POC concentrations fell within the range of this fit. The assumption of a constant POC/c_{p660} ratio close to the value suggested by Graff et al. (2015), is less likely to impact the derivation of apparent POC standing stocks and associated NCP estimates. Based on relatively small changes in b_{bp} slope values (Figs. S3d, S5d) and phytoplankton community composition, it is unlikely that changes in particle size and bulk refractive index would have significantly shifted the relationship between POC and c_{p660} during drifter deployment 2.

As concentrations of POC at drifter station 1 were 25% higher than the empirical limits of the c_p-based algorithm in (Graff et al., 2015), a different POC/c_p relationship (i.e., different slope of the linear fit) could apply. In a limited comparison with discrete POC samples, we found a POC–c_p slope that was similar to that of Graff et al. (albeit with a different y intercept) (Fig. S2). Nonetheless, we cannot rule out changes in the c_{p660}–[POC] relationship due to shifts in cell size and, to a lesser extent, bulk refractive index resulting from diatom accumulation (Kheireddine and Antoine, 2014; Stramski and Reynolds, 1993) (Fig. S3d–e). Indeed, Briggs et al. (2018) observed that the ratio of [POC] to c_p decreased by ~20% during the rise of the North Atlantic bloom, while values increased by ~60% during the bloom decline. If we assume a 20% decrease in POC/c_{p660} values (from ~420 to ~340 mg m^{-2}) associated with diatom growth (Briggs et al., 2018), our daily NCP_{POC} estimates would be closer to 0, less positive during day 1 and less negative during days 2–3. This, in turn, would increase the apparent decoupling between NCP_{POC} and $NCP_{O2/Ar}$ on days one (~27%) and three (~1%), and bring the values slightly closer on day two (~8%). Overall, the value of these potential changes is small relative to the differences we observed between $NCP_{O2/Ar}$ and NCP_{POC}, and we thus conclude that variable POC/c_{p660} ratios cannot explain the observed decoupling between POC, C_{ph} and dissolved O_2 dynamics at the drifter 1 site.

Finally, error associated with the POC mixing correction could affect calculated NCP_{POC} values (Eq. 8) and therefore the discrepancy between $NCP_{O2/Ar}$ and NCP_{POC}, and derived export estimates. This vertical mixing correction for NCP_{POC} is based on average parameters derived from N_2O measurements for the whole drifter period (Sect. 2.5). This introduces some error in day-to-day corrections to the NCP_{POC} calculations. In addition, the gradient term dPOC/dz in Eq. 10 is based on the difference between average POC concentrations measured at two depths during CTD deployments (5 m and one depth over 40-60 m). Because high-resolution transmissivity profiles showed that particle concentrations reached a steady minimum between 30 m and 40 m in most CTD deployments, dz in Eq. 10 was taken as the difference between the drifter 1 z_{mld} and this daily average depth of minimum transmissivity, rather than the deeper POC sampling depth (i.e., 40 – 60 m). Because variations in transmissivity do not necessarily equate to variations in [POC], errors in dz would impact the vertical mixing correction and therefore calculated NCP_{POC} values. For example, if the [POC] minimum was actually deeper, this would increase the value of dz and decrease dPOC/dz and the total mixing correction, yielding lower

933 NCP_{POC} values and a higher discrepancy between NCP measures. In propagating the error for
934 NCP_{POC}, we have included the standard deviation of the minimum transmissivity depth across
935 daily CTD casts, which partially addresses this uncertainty in the dz term. Fortunately, the
936 NCP_{POC} mixing corrections over drifter period 1 approximate the magnitude of the $NCP_{O2/Ar}$
937 mixing correction (Sect. 3.3, Table 1), increasing our confidence in the POC mixing correction
938 applied here.
939 Aside from uncertainties that directly impact estimates of NCP, there are a number of
940 other potential caveats in our analysis of phytoplankton carbon from b_{bp} and particle size
941 distribution from b_{bp} slope. Previous studies have reported that daily variations in b_{bp} do not
942 always track daily variations in c_p, suggesting that b_{bp} dynamics do not reflect phytoplankton
943 carbon dynamics on diel time scales (Kheireddine and Antoine, 2014; Briggs et al. 2018). We
944 observed a similar decoupling between b_{bp} and c_p in this study; for example, while c_p values at
945 660 nm steadily declined in the last 24 hours of drifter period 1, b_{bp} at 470 nm stayed relatively
946 constant. Nonetheless, [C_{ph}] estimates from b_{bp} (Fig. 2) remain useful for comparisons between
947 drifter sites, and differences in apparent phytoplankton biomass concentration were consistent
948 with a number of the other biogeochemical differences measured between the two trophic
949 regimes. Similarly, the relationship between b_{bp} slope and particle size distribution has been
950 challenged in previous literature (e.g., Zeng et al., 2018). While this limits our interpretation of
951 daily b_{bp} slope dynamics, we did find independent evidence for larger particle sizes at drifter site
952 1 (as predicted by the b_{bp} slope), from size fractionated Chl-a measurements and pigment
953 analysis showing a greater fraction of diatoms (Sect. 3.2).
954
955 **4.3 Reconciling NCP and NPP**
956
957 During both drifter surveys, we estimated daily-integrated net primary productivity
958 (NPP) values using carbon-based productivity model (CbPM) calculations and ^{14}C bottle
959 incubations (Sect. 2.5). On several days, these two measures of NPP estimates were consistently
960 lower than $NCP_{O2/Ar}$ integrated over the same time scales and mixed layer depths (Table 1; Fig.
961 4). Similarly, Briggs et al. (2018) and Alkire et al. (2012) also reported NCP values that were
962 equal to or greater than NPP values obtained from different methodologies during their
963 Lagrangian study of the North Atlantic Bloom.

In theory, NCP cannot exceed NPP, as NCP includes additional respiration terms not included in NPP, and must always be equal to or (more realistically) lower than NPP. Recent work in the Northeast Pacific Ocean, has reported mean NCP/NPP ratios, based on $\Delta O_2/Ar$ measurements and CbPM calculations, in the 0.16 to 0.26 range for offshore and coastal waters, respectively (Burt et al., 2018). These values, determined from continuous observations along a moving ship-track are consistent with theoretical expectations. The observed high (>1) apparent NCP/NPP values observed in our study and that of Briggs et al. (2018) and Alkire et al. (2012) highlight a number of methodological limitations that could depress NPP estimates.

One possibility, which has been discussed at length by various authors (Gieskes et al., 1979; Fogg and Calvario-Martinez, 1989; Marra, 2009), is that bottle containment effects limit accurate estimates of ^{14}C uptake. This likely caused underestimates of ^{14}C-NPP during both drifter surveys, relative to CbPM-NPP and $NCP_{O2/Ar}$, which do not require discrete sample incubations. In addition, during this last ^{14}C-uptake experiment of drifter survey 2, the incubator warmed, which could have significantly impacted phytoplankton growth rates during the incubation and result in depressed ^{14}C-NPP values, if thermal optima were exceeded.

A number of factors may also depress CbPM-based NPP estimates. While the model applies a satellite-based relationship between [Chl-a]/[C_{ph}] and daily mixed layer irradiance (E_g) to calculate growth rate, these E_g values may not fully parametrize phytoplankton physiology for mixed assemblages in the ocean (Westberry et al., 2008). Indeed, phytoplankton photophysiology varies with other environmental conditions and phytoplankton composition (Cloern et al., 1995; Geider et al., 1998; MacIntyre et al., 2002; Westberry et al., 2008). In addition, the CbPM does not allow calculated growth rates to exceed 2 d^{-1}, which may not apply to all ocean environments (Graff et al., 2016). These uncertainties could potentially impact the applicability of the CbPM parameters to the specific ocean conditions at drifter sites 1 and 2. In addition, a vertical mixing correction for ac-s and backscatter-derived [Chl-a] and [C_{ph}], respectively, not feasible in the present data set, may improve CbPM-based estimates of NPP.

4.4 Comparison to other studies

A number of previous studies have examined diurnal variation in upper ocean phytoplankton and organic particle dynamics across a variety of productivity regimes, from

oligotrophic environments (Claustre et al., 1999, 2008; Wu et al., 2010; Gernez et al., 2011; Kheireddine and Antoine, 2014; Thyssen et al., 2014; Nicholson et al., 2015; Ribalet et al., 2015; White et al., 2017), to higher productivity waters and phytoplankton blooms (Brunet and Lizon, 2003; Wu et al., 2010; Alkire et al., 2012; Gernez et al., 2011; Dugenne et al., 2014; Kheireddine and Antoine, 2014; Needham and Fuhrman, 2016; Briggs et al., 2018). In general, these studies have shown that more productive environments exhibit higher amplitude diurnal variations in beam attenuation, POC concentration, phytoplankton cell abundances, Chl-a, and metabolic rates, as compared to oligotrophic regions. These prior results are consistent with the differences we observed between the two distinct Northeast Pacific trophic environments represented by drifter sites 1 and 2, respectively (Sect. 3.2; Figs. 2, S5).

To our knowledge, however, only two previous studies have directly compared diurnal variations in O_2-based and c_p-based mixed layer productivity using Lagrangian drifters (Alkire et al., 2012; Briggs et al., 2018). This previous work demonstrated that GPP and NCP dynamics derived from dissolved O_2 measurements differed from net POC accumulation over the course of the North Atlantic bloom, with the magnitude of this disparity varying as a function of bloom stage. The authors found that highest rates of POC export and DOC production, corresponding to the greatest O_2-POC discrepancy, occurred during the main period of the bloom development, prior to its termination. The results of our study off the Oregon coast extend these previous observations from the North Atlantic bloom into two new surface ocean regimes: a high productivity Pacific upwelling zone, and a lower productivity offshore region. The upwelling environment was characterized by rapid diatom accumulation, yielding significant differences between $NCP_{O2/Ar}$ and NCP_{POC}, and $GPP_{O2/Ar}$ and GPP_{POC}. We also observed significant differences between $\Delta O_2/Ar$-based and POC-based GPP and CR rates at the lower productivity drifter 2 site, even though daily-integrated measures of NCP and net carbon accumulation agreed more closely.

While most previous work across oligotrophic environments has highlighted the agreement between GPP derived from daily variability in beam attenuation and dissolved O_2 (e.g., Claustre et al., 2008; White et al., 2017), our results illustrate two different examples where $\Delta O_2/Ar$-based and POC-based GPP rates do not agree. We have found that even lower productivity environments like drifter site 2 can display a quantifiable discrepancy between productivity measures. At this site, even though POC-derived GPP and CR consistently

underestimated $\Delta O_2/Ar$-derived rates, net changes in [POC] were a sufficient relative indicator of variations in $\Delta O_2/Ar$-based productivity, as has been observed in previous work (Briggs et al., 2018). As a result, NCP measures agreed well, supporting the continued use of diurnal measurements of beam attenuation to estimate NCP_{POC} in low productivity regimes, where POC and O_2 dynamics are closely coupled. In higher productivity regions like at drifter site 1 or the area of the North Atlantic Bloom (Alkire et al., 2012; Briggs et al., 2018), measurements of both POC and O_2 are likely required to constrain organic carbon mass balance, where POC and O_2 dynamics can be significantly uncoupled on short time scales. Measurements that simultaneously estimate surface water O_2 accumulation, net DOC production and vertical transport of deep water to the mixed layer at high temporal resolution offer the opportunity to evaluate the fate of NCP. These quantities are especially important in the California coastal upwelling regime and other similar ecosystems, with high NCP and significant potential for carbon transfer to higher trophic levels.

5 Conclusions

In the current study, biological oxygen saturation ($\Delta O_2/Ar$) and optically-derived particulate organic carbon (POC) were measured continuously and simultaneously during two Lagrangian drifter deployments. This dual measurement approach allowed us to examine the (de)coupling between carbon and dissolved oxygen in surface waters, and facilitated direct comparison of O_2/Ar and POC-derived measures of gross primary productivity (GPP), community respiration (CR), and net community production (NCP), from a mesotrophic upwelling-influenced system to a more oligotrophic system further offshore. As hypothesized, the results show that O_2 and POC-based measures of GPP and NCP diverge in mid-to-high productivity phytoplankton communities, where daily fluctuations in $\Delta O_2/Ar$ are decoupled from POC cycling. Interestingly, oxygen-based GPP and CR exceeded POC-based GPP and CR rates at the lower productivity site too, though we found that net changes in POC scaled with changing productivity based on $\Delta O_2/Ar$. Thus, NCP estimates at drifter site 2 showed better agreement because O_2 and POC cycles appeared to be more tightly coupled.

These findings are generally consistent with current understanding of productivity dynamics and mixed layer POC cycling in these two coastal Pacific environments, and

complement only one prior comparison of daily GPP and NCP estimates from simultaneous, autonomous measurements of c_p and O_2 in the North Atlantic mixed layer (Alkire et al., 2012; Briggs et al., 2018). Importantly, however, our results differ from earlier studies by providing two examples of significant disagreement between $GPP_{O2/Ar}$ and GPP_{POC}, and $CR_{O2/Ar}$ and CR_{POC} rates. We have further shown that for upwelling regions like drifter site 1, it is important to account for vertical mixing of sub-surface waters into the mixed layer, and its effect on not only $NCP_{O2/Ar}$ calculations (Izett et al., 2018), but also on NCP_{POC} estimates through dilution of the surface POC signature. Thus, our study illustrates an application of the vertical mixing coefficient, k_{mix}, derived from [N_2O] profiles, to more accurately estimate net changes in POC and nutrient concentration in such environments.

Moving forward, the disparity between POC and O_2-based NCP estimates offers an opportunity to continuously track cumulative POC losses in the mixed layer using autonomous ship-board or in situ sensors. The results show that this approach performs well in distinguishing regions of high particle export, notwithstanding some major methodological limitations (Sect. 4.2) and poorly constrained DOC production rates (Sect. 4.1.1), which increase the uncertainty of our export estimates at drifter site 1. As it is difficult and labor intensive to measure POC export on short time scales with sediment traps and the ^{234}Th-^{238}U disequilibrium method (Buesseler et al., 2006; Savoye et al., 2006), simultaneous underway measurements of dissolved O_2, particulate beam attenuation and CDOM absorption and spectral slope over a range of wavelengths <400 nm (Del Vecchio and Blough, 2004; Grunert et al., 2018) may provide a valuable, first-order approximation of POC partitioning among living phytoplankton biomass, particle export and dissolved organic carbon (DOC) in the surface ocean on short time scales.

For future work, we recommend a number of approaches to increase our confidence in derived POC export from coupled O_2, POC, and DOC dynamics. First, it will be valuable to constrain particle size, and partitioning of POC into detrital and living (phytoplankton and heterotrophic bacteria) components to properly assess the size range captured by optics-based POC and C_{ph} measurements. Second, independent estimates of POC export and DOC concentrations during each drifter deployment could validate estimates of POC export fluxes derived from coupled O_2 and POC measurements. Relatedly, depth-resolved backscatter profiles (Briggs et al., 2013, 2018) could be used as another autonomous approach to calculating export fluxes, as an independent check on surface-based estimates. Going forward, there is significant

future potential to exploit coupled O_2 and c_p measurements on autonomous platforms, including various ocean moorings (e.g., the Optical Dynamics Experiment, the Biowatt II program, and the Bermuda Testbed Mooring program), and biogeochemical floats and gliders to resolve opportunistic, high-resolution POC export time series (Stramska and Dickey, 1992; Kinkade et al., 1999; Dickey and Chang, 2002). Deployment of such autonomous measurement systems across a range of oceanic regions will help to constrain POC and productivity dynamics on global scales.

Data availability

Discrete and underway optical measurements may be accessed at https://github.com/srosengard/rosengard-tortell-oc2017.git

Author contributions

Sarah Rosengard, Philippe Tortell, and Nina Schuback collected the data in the field. Robert Izett processed the CTD cast data and nitrous oxide measurements. Sarah Rosengard wrote the manuscript with significant input from the co-authors.

Competing interests

The authors declare that they have no conflict of interest.

Acknowledgements

Special thanks to Jessie Gwinn, Jay Pinckney, Ross McCulloch, Chen Zeng, Melissa Beaulac, Chris Payne and Maureen Soon for assistance in field collection and analysis of samples, and to two anonymous reviewers for greatly strengthening the interpretations in this manuscript. This project was funded by the Natural Sciences and Engineering Research Council of Canada (NSERC), and by the US National Science Foundation (NSF project number 1436344).

References

Alkire, M. B., D'Asaro, E., Lee, C., Jane Perry, M., Gray, A., Cetinić, I., Briggs, N., Rehm, E., Kallin, E., Kaiser, J. and González-Posada, A.: Estimates of net community production and export using high-resolution, Lagrangian measurements of O2, NO3−, and POC through the evolution of a spring diatom bloom in the North Atlantic, Deep Sea Res. Part I Oceanogr. Res. Pap., 64, 157–174, doi:10.1016/j.dsr.2012.01.012, 2012.

Barnes, M., and Antoine, D.: Proxies of community production derived from the diel variability of particulate attenuation and backscattering coefficients in the northwest Mediterranean Sea, Limnol. Oceanogr., 59(6), 2133-2149, 2014.

Behrenfeld, M. J., Boss, E., Siegel, D. A. and Shea, D. M.: Carbon-based ocean productivity and phytoplankton physiology from space, Global Biogeochem. Cycles, 19(1), 2005.

Bif, M. B. and Hansell, D. A.: Seasonality of dissolved organic carbon in the upper Northeast Pacific Ocean, Global Biogeochem. Cycles, 2019.

Bif, M. B., Hansell, D. A. and Popendorf, K. J.: Controls on the fate of dissolved organic carbon under contrasting upwelling conditions, Front. Mar. Sci., 5, 463, 2018.

Boss, E., Twardowski, M. S. and Herring, S.: Shape of the particulate beam attenuation spectrum and its inversion to obtain the shape of the particulate size distribution, Appl. Opt., 40(27), 4885–4893, 2001.

de Boyer Montégut, C., Madec, G., Fischer, A. S., Lazar, A. and Iudicone, D.: Mixed layer depth over the global ocean: An examination of profile data and a profile-based climatology, J. Geophys. Res., 109(C12), C12003, doi:10.1029/2004JC002378, 2004.

Briggs, N., Guðmundsson, K., Cetinić, I., D'Asaro, E., Rehm, E., Lee, C. and Perry, M. J.: A multi-method autonomous assessment of primary productivity and export efficiency in the springtime North Atlantic, Biogeosciences, 15(14), 4515–4532, 2018.

Briggs, N. T., Slade, W. H., Boss, E. and Perry, M. J.: Method for estimating mean particle size from high-frequency fluctuations in beam attenuation or scattering measurements, Appl. Opt., 52(27), 6710–6725, 2013.

Brunet, C. and Lizon, F.: Tidal and diel periodicities of size-fractionated phytoplankton pigment signatures at an offshore station in the southeastern English Channel, Estuar. Coast. Shelf Sci., 56(3–4), 833–843, 2003.

Brzezinski, M., Villareal, T. and Lipschultz, F.: Silica production and the contribution of diatoms to new and primary production in the central North Pacific, Mar. Ecol. Prog. Ser., 167, 89–104, doi:10.3354/meps167089, 1998.

Brzezinski, M. A.: The Si:C:N ratio of marine diatoms: Interspecific variability and the effect of some environmental variables, J. Phycol., 21(3), 347–357, doi:10.1111/j.0022-3646.1985.00347.x, 2004.

Brzezinski, M. A., Krause, J. W., Bundy, R. M., Barbeau, K. A., Franks, P., Goericke, R., Landry, M. R. and Stukel, M. R.: Enhanced silica ballasting from iron stress sustains carbon export in a frontal zone within the California Current, J. Geophys. Res. Ocean., 120(7), 4654–4669, 2015.

Buesseler, K. O.: The decoupling of production and particulate export in the surface ocean, Global Biogeochem. Cycles, 12(2), 297–310, 1998.

Buesseler, K. O., Benitez-Nelson, C. R., Moran, S. B., Burd, A., Charette, M., Cochran, J. K., Coppola, L., Fisher, N. S., Fowler, S. W. and Gardner, W. D.: An assessment of particulate organic carbon to thorium-234 ratios in the ocean and their impact on the application of 234Th as a POC flux proxy, Mar. Chem., 100(3–4), 213–233, 2006.

Burt, W. J. and Tortell, P. D.: Observations of Zooplankton Diel Vertical Migration From High-Resolution Surface Ocean Optical Measurements, Geophys. Res. Lett., 45(24), 13–396, 2018.

Burt, W. J., Westberry, T. K., Behrenfeld, M. J., Zeng, C., Izett, R. W. and Tortell, P. D.: Carbon: Chlorophyll Ratios and Net Primary Productivity of Subarctic Pacific Surface Waters Derived From Autonomous Shipboard Sensors, Global Biogeochem. Cycles, 32(2), 267–288, doi:10.1002/2017GB005783, 2018.

Capelle, D. W., Dacey, J. W. and Tortell, P. D.: An automated, high through-put method for accurate and precise measurements of dissolved nitrous-oxide and methane concentrations in natural waters, Limnol. Oceanogr. Methods, 13(7), 345–355, 2015.

Cassar, N., Barnett, B. A., Bender, M. L., Kaiser, J., Hamme, R. C. and Tilbrook, B.: Continuous high-frequency dissolved O2/Ar measurements by equilibrator inlet mass spectrometry, Anal. Chem., 81(5), 1855–1864, 2009.

Cassar, N., Nevison, C. D. and Manizza, M.: Correcting oceanic O2/Ar-net community production estimates for vertical mixing using N2O observations, Geophys. Res. Lett., 41(24), 8961–8970, 2014.

Charette, M. A., Moran, S. B. and Bishop, J. K. B.: 234Th as a tracer of particulate organic carbon export in the subarctic northeast Pacific Ocean, Deep Sea Res. Part II Top. Stud. Oceanogr., 46(11-12), 2833-2861, 1999.

Church, M. J., Ducklow, H. W., and Karl, D. M.: Light dependence of [3H] leucine incorporation in the oligotrophic North Pacific Ocean, Appl. Environ. Microbiol., 70(7), 4079-4087, 2004.

Claustre, H., Morel, A., Babin, M., Cailliau, C., Marie, D., Marty, J., Tailliez, D. and Vaulot, D.: Variability in particle attenuation and chlorophyll fluorescence in the tropical Pacific: Scales, patterns, and biogeochemical implications, J. Geophys. Res. Ocean., 104(C2), 3401–3422, 1999.

Claustre, H., Huot, Y., Obernosterer, I., Gentili, B., Tailliez, D. and Lewis, M.: Gross community production and metabolic balance in the South Pacific Gyre, using a non intrusive bio-optical method, Biogeosciences, 5, 463-474, 2008.

Cloern, J. E., Grenz, C. and Vidergar-Lucas, L.: An empirical model of the phytoplankton chlorophyll: carbon ratio-the conversion factor between productivity and growth rate, Limnol. Oceanogr., 40(7), 1313–1321, 1995.

Dagg, M. J., Vidal, J., Whitledge, T. E., Iverson, R. L. and Goering, J. J.: The feeding, respiration, and excretion of zooplankton in the Bering Sea during a spring bloom, Deep Sea Res. Part A. Oceanogr. Res. Pap., 29(1), 45–63, 1982.

Dall'Olmo, G., Boss, E., Behrenfeld, M. J., Westberry, T. K., Courties, C., Prieur, L., Pujo-Pay, M., Hardman-Mountford, N. and Moutin, T.: Inferring phytoplankton carbon and eco-physiological rates from diel cycles of spectral particulate beam-attenuation coefficient, Biogeosciences, 8(11), 3423–3439, 2011.

Del Vecchio, R., and Blough, N. V.: Spatial and seasonal distribution of chromophoric dissolved organic matter and dissolved organic carbon in the Middle Atlantic Bight, Mar. Chem., 89(1-4), 169-187, 2004.

Dickey, T. D. and Chang, G. C.: Recent advances and future visions: temporal variability of optical and bio-optical properties of the ocean, Oceanogr. DC-OCEANOGRAPHY Soc., 14(3), 15–29, 2002.

Dugenne, M., Thyssen, M., Nerini, D., Mante, C., Poggiale, J.-C., Garcia, N., Garcia, F. and Grégori, G. J.: Consequence of a sudden wind event on the dynamics of a coastal phytoplankton community: an insight into specific population growth rates using a single cell high frequency

approach, Front. Microbiol., 5, 485, 2014.
Durand, M. D., and Olson, R. J.: Contributions of phytoplankton light scattering and cell concentration changes to diel variations in beam attenuation in the equatorial Pacific from flow cytometric measurements of pico-, ultra-and nanoplankton, Deep Sea Res. Part II Top. Stud. Oceanogr., 43(4-6), 891-906, 1996.
Durkin, C. A., Estapa, M. L. and Buesseler, K. O.: Observations of carbon export by small sinking particles in the upper mesopelagic, Mar. Chem., 175, 72–81, doi:10.1016/J.MARCHEM.2015.02.011, 2015.
Ferrón, S., Wilson, S. T., Martínez-García, S., Quay, P. D., and Karl, D. M.: Metabolic balance in the mixed layer of the oligotrophic North Pacific Ocean from diel changes in O2/Ar saturation ratios, Geophys. Res. Lett., 42(9), 3421-3430, 2015.
Fogg, G. E. and Calvario-Martinez, O.: Effects of bottle size in determinations of primary productivity by phytoplankton, Hydrobiologia, 173(2), 89–94, doi:10.1007/BF00015518, 1989.
Fowler, S. W. and Knauer, G. A.: Role of large particles in the transport of elements and organic compounds through the oceanic water column, Prog. Oceanogr., 16(3), 147–194, doi:10.1016/0079-6611(86)90032-7, 1986.
Fuhrman, J. A., Eppley, R. W., Hagström, Å., and Azam, F.: Diel variations in bacterioplankton, phytoplankton, and related parameters in the Southern California Bight, Mar. Ecol. Prog. Ser, 27, 9-20, 1985.
Garcia, H. E. and Gordon, L. I.: Oxygen solubility in seawater: Better fitting equations, Limnol. Oceanogr., 37(6), 1307–1312, 1992.
Gardner, W. D., Walsh, I. D. and Richardson, M. J.: Biophysical forcing of particle production and distribution during a spring bloom in the North Atlantic, Deep Sea Res. Part II Top. Stud. Oceanogr., 40(1–2), 171–195, 1993.
Geider, R. J., Maclntyre, H. L. and Kana, T. M.: A dynamic regulatory model of phytoplanktonic acclimation to light, nutrients, and temperature, Limnol. Oceanogr., 43(4), 679–694, 1998.
Gernez, P., Antoine, D. and Huot, Y.: Diel cycles of the particulate beam attenuation coefficient under varying trophic conditions in the northwestern Mediterranean Sea: Observations and modeling, Limnol. Oceanogr., 56(1), 17–36, 2011.
Gieskes, W. W. C., Kraay, G. W. and Baars, M. A.: Current 14C methods for measuring primary production: Gross underestimates in oceanic waters, Netherlands J. Sea Res., 13(1), 58–78,

doi:10.1016/0077-7579(79)90033-4, 1979.
Graff, J. R., Westberry, T. K., Milligan, A. J., Brown, M. B., Dall'Olmo, G., Dongen-Vogels, V. van, Reifel, K. M. and Behrenfeld, M. J.: Analytical phytoplankton carbon measurements spanning diverse ecosystems, Deep Sea Res. Part I Oceanogr. Res. Pap., 102, 16–25, doi:10.1016/J.DSR.2015.04.006, 2015.
Graff, J. R., Westberry, T. K., Milligan, A. J., Brown, M. B., Olmo, G. D., Reifel, K. M. and Behrenfeld, M. J.: Photoacclimation of natural phytoplankton communities, Mar. Ecol. Prog. Ser., 542, 51–62, 2016.
Grunert, B. K., Mouw, C. B., and Ciochetto, A. B.: Characterizing CDOM spectral variability across diverse regions and spectral ranges, Global Biogeochem. Cycles, 32(1), 57-77, 2018.
Guidi, L., Jackson, G. A., Stemmann, L., Carlos Miquel, J., Picheral, M. and Gorsky, G.: Author's personal copy Relationship between particle size distribution and flux in the mesopelagic zone, , doi:10.1016/j.dsr.2008.05.014, 2008.
Guidi, L., Stemmann, L., Jackson, G. A., Ibanez, F., Claustre, H., Legendre, L., Picheral, M. and Gorskya, G.: Effects of phytoplankton community on production, size, and export of large aggregates: A world-ocean analysis, Limnol. Oceanogr., 54(6), 1951–1963, 2009.
Hamme, R. C., Cassar, N., Lance, V. P., Vaillancourt, R. D., Bender, M. L., Strutton, P. G., Moore, T. S., DeGrandpre, M. D., Sabine, C. L. and Ho, D. T.: Dissolved O2/Ar and other methods reveal rapid changes in productivity during a Lagrangian experiment in the Southern Ocean, J. Geophys. Res. Ocean., 117(C4), 2012.
Hansell, D. A. and Carlson, C. A.: Net community production of dissolved organic carbon, Global Biogeochem. Cycles, 12(3), 443–453, 1998.
Henson, S. A., Sanders, R. and Madsen, E.: Global patterns in efficiency of particulate organic carbon export and transfer to the deep ocean, Global Biogeochem. Cycles, 26(1), 2012.
Hickey, B. M., Pietrafesa, L. J., Jay, D. A. and Boicourt, W. C.: The Columbia River plume study: Subtidal variability in the velocity and salinity fields, J. Geophys. Res. Ocean., 103(C5), 10339–10368, 1998.
Hirata, T., Hardman-Mountford, N. J., Brewin, R. J. W., Aiken, J., Barlow, R., Suzuki, K., Isada, T., Howell, E., Hashioka, T. and Noguchi-Aita, M.: Synoptic relationships between surface Chlorophyll-a and diagnostic pigments specific to phytoplankton functional types, Biogeosciences, 8(2), 311–327, 2011.

Hopkinson, B. M., and Barbeau, K.A.: Organic and redox speciation of iron in the eastern tropical North Pacific suboxic zone, Mar. Chem., 106(1-2), 2-17, 2007.

Hoppe, C. J. M., Schuback, N., Semeniuk, D. M., Maldonado, M. T. and Rost, B.: Functional Redundancy Facilitates Resilience of Subarctic Phytoplankton Assemblages toward Ocean Acidification and High Irradiance , Front. Mar. Sci. , 4, 229 [online] Available from: https://www.frontiersin.org/article/10.3389/fmars.2017.00229, 2017.

Izett, R. W., Manning, C. C., Hamme, R. C. and Tortell, P. D.: Refined estimates of net community production in the Subarctic Northeast Pacific derived from ΔO2/Ar measurements with N2O-based corrections for vertical mixing, Global Biogeochem. Cycles, 32(3), 326–350, 2018.

Jin, X., Najjar, R. G., Louanchi, F. and Doney, S. C.: A modeling study of the seasonal oxygen budget of the global ocean, J. Geophys. Res. Ocean., 112(C5), 2007.

Kaiser, J., Reuer, M. K., Barnett, B. and Bender, M. L.: Marine productivity estimates from continuous O2/Ar ratio measurements by membrane inlet mass spectrometry, Geophys. Res. Lett., 32(19), 2005.

Karl, D. M., Hebel, D. V., Björkman, K., and Letelier, R. M.: The role of dissolved organic matter release in the productivity of the oligotrophic North Pacific Ocean, Limnol. Oceanogr., 43(6), 1270-1286, 1998.

Keeling, R. F. and Shertz, S. R.: Seasonal and interannual variations in atmospheric oxygen and implications for the global carbon cycle, Nature, 358(6389), 723, 1992.

Kheireddine, M. and Antoine, D.: Diel variability of the beam attenuation and backscattering coefficients in the northwestern Mediterranean Sea (BOUSSOLE site), J. Geophys. Res. Ocean., 119(8), 5465–5482, 2014.

Kinkade, C. S., Marra, J., Dickey, T. D., Langdon, C., Sigurdson, D. E. and Weller, R.: Diel bio-optical variability observed from moored sensors in the Arabian Sea, Deep sea Res. Part II Top. Stud. Oceanogr., 46(8–9), 1813–1831, 1999.

Kostadinov, T. S., Siegel, D. A. and Maritorena, S.: Retrieval of the particle size distribution from satellite ocean color observations, J. Geophys. Res., 114(C9), C09015, doi:10.1029/2009JC005303, 2009.

Kuipers, B., van Noort, G. J., Vosjan, J., and Herndl, G. J.: Diel periodicity of bacterioplankton in the euphotic zone of the subtropical Atlantic Ocean, Mar. Ecol. Prog. Ser., 201, 13-25, 2000.

Laws, E. A.: Photosynthetic quotients, new production and net community production in the open ocean, Deep Sea Res. Part A. Oceanogr. Res. Pap., 38(1), 143–167, 1991.
Lide, D. R.: Physical and optical properties of minerals, CRC Handb. Chem. Phys., 4–130, 1997.
Lochte, K., Ducklow, H. W., Fasham, M. J. R. and Stienen, C.: Plankton succession and carbon cycling at 47 N 20 W during the JGOFS North Atlantic Bloom Experiment, Deep Sea Res. Part II Top. Stud. Oceanogr., 40(1–2), 91–114, 1993.
Loisel, H., Nicolas, J.-M., Sciandra, A., Stramski, D. and Poteau, A.: Spectral dependency of optical backscattering by marine particles from satellite remote sensing of the global ocean, J. Geophys. Res., 111(C9), C09024, doi:10.1029/2005JC003367, 2006.
MacIntyre, H. L., Kana, T. M., Anning, T. and Geider, R. J.: Photoacclimation of irradiance response curves and photosynthetic pigments in microalgae and cyanobacteria, J. Phycol., 38(1), 17–38, doi:10.1046/j.1529-8817.2002.00094.x, 2002.
Manning, C. C., Stanley, R. H. R., Nicholson, D. P., Smith, J. M., Pennington, J. T., Fewings, M. R., Squibb, M. E. and Chavez, F. P.: Impact of recently upwelled water on productivity investigated using in situ and incubation-based methods in Monterey Bay, J. Geophys. Res. Ocean., 122(3), 1901–1926, 2017.
Marra, J.: Approaches to the measurement of plankton production, Phytoplankt. Product. Carbon Assim. Mar. Freshw. Ecosyst., 78–108, 2002.
Marra, J.: Net and gross productivity: weighing in with 14C, Aquat. Microb. Ecol., 56(2–3), 123–131, doi:10.3354/ame01306, 2009.
Morel, A., Huot, Y., Gentili, B., Werdell, P. J., Hooker, S. B. and Franz, B. A.: Examining the consistency of products derived from various ocean color sensors in open ocean (Case 1) waters in the perspective of a multi-sensor approach, Remote Sens. Environ., 111(1), 69–88, 2007.
Murphy, J. and Riley, J. P.: A modified single solution method for the determination of phosphate in natural waters, Anal. Chim. Acta, 27, 31–36, 1962.
Needham, D. M. and Fuhrman, J. A.: Pronounced daily succession of phytoplankton, archaea and bacteria following a spring bloom, Nat. Microbiol., 1(4), 16005, 2016.
Nicholson, D. P., Wilson, S. T., Doney, S. C. and Karl, D. M.: Quantifying subtropical North Pacific gyre mixed layer primary productivity from Seaglider observations of diel oxygen cycles, Geophys. Res. Lett., 42(10), 4032–4039, 2015.
Organelli, E., Bricaud, A., Antoine, D. and Matsuoka, A.: Seasonal dynamics of light absorption

by chromophoric dissolved organic matter (CDOM) in the NW Mediterranean Sea (BOUSSOLE site), Deep Sea Res. Part I Oceanogr. Res. Pap., 91, 72–85, 2014.
Oubelkheir, K., and Sciandra, A.: Diel variations in particle stocks in the oligotrophic waters of the Ionian Sea (Mediterranean), J. Marine Syst., 74(1-2), 364-371, 2008.
Peacock, M., Evans, C. D., Fenner, N., Freeman, C., Gough, R., Jones, T. G. and Lebron, I.: UV-visible absorbance spectroscopy as a proxy for peatland dissolved organic carbon (DOC) quantity and quality: considerations on wavelength and absorbance degradation, Environ. Sci. Process. Impacts, 16(6), 1445–1461, 2014.
Raymond, P. A., Zappa, C. J., Butman, D., Bott, T. L., Potter, J., Mulholland, P., Laursen, A. E., McDowell, W. H. and Newbold, D.: Scaling the gas transfer velocity and hydraulic geometry in streams and small rivers, Limnol. Oceanogr. Fluids Environ., 2(1), 41–53, 2012.
Reuer, M. K., Barnett, B. A., Bender, M. L., Falkowski, P. G. and Hendricks, M. B.: New estimates of Southern Ocean biological production rates from O2/Ar ratios and the triple isotope composition of O2, Deep Sea Res. Part I Oceanogr. Res. Pap., 54(6), 951–974, 2007.
Ribalet, F., Swalwell, J., Clayton, S., Jiménez, V., Sudek, S., Lin, Y., Johnson, Z. I., Worden, A. Z. and Armbrust, E. V.: Light-driven synchrony of Prochlorococcus growth and mortality in the subtropical Pacific gyre, Proc. Natl. Acad. Sci., 112(26), 8008–8012, 2015.
Riley, J. P.: Grasshoff, K. [Ed.] 1976. Methods of seawater analysis. Verlag Chemie, Weinheim and New York, xv+ 317 p. $43.60., 1977.
Roesler, C. S. and Barnard, A. H.: Optical proxy for phytoplankton biomass in the absence of photophysiology: Rethinking the absorption line height, Methods Oceanogr., 7, 79–94, 2013.
Savoye, N., Benitez-Nelson, C., Burd, A. B., Cochran, J. K., Charette, M., Buesseler, K. O., Jackson, G. A., Roy-Barman, M., Schmidt, S. and Elskens, M.: 234Th sorption and export models in the water column: a review, Mar. Chem., 100(3–4), 234–249, 2006.
Schuback, N., Flecken, M., Maldonado, M. T. and Tortell, P. D.: Diurnal variation in the coupling of photosynthetic electron transport and carbon fixation in iron-limited phytoplankton in the NE subarctic Pacific, Biogeosciences, 13, 1019–1035, doi:10.5194/bg-13-1019-2016, 2016.
Siegel, D. A., Dickey, T. D., Washburn, L., Hamilton, M. K. and Mitchell, B. G.: Optical determination of particulate abundance and production variations in the oligotrophic ocean, Deep Sea Res. Part A. Oceanogr. Res. Pap., 36(2), 211–222, 1989.

Stanley, R. H. R., Kirkpatrick, J. B., Cassar, N., Barnett, B. A. and Bender, M. L.: Net community production and gross primary production rates in the western equatorial Pacific, Global Biogeochem. Cycles, 24(4), 2010.

Stramska, M. and Dickey, T. D.: Short-term variations of the bio-optical properties of the ocean in response to cloud-induced irradiance fluctuations, J. Geophys. Res. Ocean., 97(C4), 5713–5721, 1992.

Stramska, M. and Dickey, T. D.: Modeling phytoplankton dynamics in the northeast Atlantic during the initiation of the spring bloom, J. Geophys. Res. Ocean., 99(C5), 10241–10253, 1994.

Stramska, M., Stramski, D., Hapter, R., Kaczmarek, S. and Ston´, J. S.: Bio-optical relationships and ocean color algorithms for the north polar region of the Atlantic, J. Geophys. Res, 108(C5), 3143, doi:10.1029/2001JC001195, 2003.

Stramski, D. and Kiefer, D. A.: Light scattering by microorganisms in the open ocean, Prog. Oceanogr., 28(4), 343–383, doi:10.1016/0079-6611(91)90032-H, 1991.

Stramski, D. and Reynolds, R. A.: Diel variations in the optical properties of a marine diatom, Limnol. Oceanogr., 38(7), 1347–1364, 1993.

Stukel, M. R., Aluwihare, L. I., Barbeau, K. A., Chekalyuk, A. M., Goericke, R., Miller, A. J., Ohman, M. D., Ruacho, A., Song, H. and Stephens, B. M.: Mesoscale ocean fronts enhance carbon export due to gravitational sinking and subduction, Proc. Natl. Acad. Sci., 114(6), 1252–1257, 2017.

Sullivan, J. M., Twardowski, M. S., Donaghay, P. L. and Freeman, S. A.: Use of optical scattering to discriminate particle types in coastal waters, Appl. Opt., 44(9), 1667, doi:10.1364/AO.44.001667, 2005.

Thomas, A. C. and Weatherbee, R. A.: Satellite-measured temporal variability of the Columbia River plume, Remote Sens. Environ., 100(2), 167–178, doi:10.1016/J.RSE.2005.10.018, 2006.

Thomson, R. E., Fine, I. V., Thomson, R. E. and Fine, I. V.: Estimating Mixed Layer Depth from Oceanic Profile Data, J. Atmos. Ocean. Technol., 20(2), 319–329, doi:10.1175/1520-0426(2003)020<0319:EMLDFO>2.0.CO;2, 2003.

Thyssen, M., Grégori, G. J., Grisoni, J.-M., Pedrotti, M. L., Mousseau, L., Artigas, L. F., Marro, S., Garcia, N., Passafiume, O. and Denis, M. J.: Onset of the spring bloom in the northwestern Mediterranean Sea: influence of environmental pulse events on the in situ hourly-scale dynamics of the phytoplankton community structure, Front. Microbiol., 5, 387, 2014.

Tortell, P. D.: Dissolved gas measurements in oceanic waters made by membrane inlet mass spectrometry, Limnol. Oceanogr. Methods, 3(1), 24–37, 2005.

Tortell, P. D., Guéguen, C., Long, M. C., Payne, C. D., Lee, P. and DiTullio, G. R.: Spatial variability and temporal dynamics of surface water pCO2, ΔO2/Ar and dimethylsulfide in the Ross Sea, Antarctica, Deep Sea Res. Part I Oceanogr. Res. Pap., 58(3), 241–259, 2011.

Tortell, P. D., Asher, E. C., Ducklow, H. W., Goldman, J. A. L., Dacey, J. W. H., Grzymski, J. J., Young, J. N., Kranz, S. A., Bernard, K. S. and Morel, F. M. M.: Metabolic balance of coastal Antarctic waters revealed by autonomous pCO2 and ΔO2/Ar measurements, Geophys. Res. Lett., 41(19), 6803–6810, 2014.

Turner, R. E., Qureshi, N., Rabalais, N. N., Dortch, Q., Justic, D., Shaw, R. F. and Cope, J.: Fluctuating silicate: nitrate ratios and coastal plankton food webs, Proc. Natl. Acad. Sci., 95(22), 13048–13051, 1998.

Twardowski, M. S., Boss, E., Macdonald, J. B., Pegau, W. S., Barnard, A. H. and Zaneveld, J. R. V.: A model for estimating bulk refractive index from the optical backscattering ratio and the implications for understanding particle composition in case I and case II waters, J. Geophys. Res. Ocean., 106(C7), 14129–14142, doi:10.1029/2000JC000404, 2001.

Waite, A. M., and Nodder, S. D.: The effect of in situ iron addition on the sinking rates and export flux of Southern Ocean diatoms, Deep Sea Res. Part II Top. Stud. Oceanogr., 48(11-12), 2635-2654, 2001.

Wanninkhof, R.: Relationship between wind speed and gas exchange over the ocean revisited, Limnol. Oceanogr. Methods, 12(6), 351–362, 2014.

Weiss, R. F. and Price, B. A.: Nitrous oxide solubility in water and seawater, Mar. Chem., 8(4), 347–359, 1980.

Westberry, T., Behrenfeld, M. J., Siegel, D. A. and Boss, E.: Carbon-based primary productivity modeling with vertically resolved photoacclimation, Global Biogeochem. Cycles, 22(2), 2008.

White, A. E., Barone, B., Letelier, R. M. and Karl, D. M.: Productivity diagnosed from the diel cycle of particulate carbon in the North Pacific Subtropical Gyre, Geophys. Res. Lett., 44(8), 3752–3760, 2017.

Whitney, F. . and Freeland, H. .: Variability in upper-ocean water properties in the NE Pacific Ocean, Deep Sea Res. Part II Top. Stud. Oceanogr., 46(11–12), 2351–2370, doi:10.1016/S0967-0645(99)00067-3, 1999.

Wu, C.-J., Chiang, K.-P. and Liu, H.: Diel feeding pattern and prey selection of mesozooplankton on microplankton community, J. Exp. Mar. Bio. Ecol., 390(2), 134–142, 2010.

Zeng, C., Rosengard, S. Z., Burt, W., Peña, M. A., Nemcek, N., Zeng, T., Arrigo, K. R. and Tortell, P. D.: Optically-derived estimates of phytoplankton size class and taxonomic group biomass in the Eastern Subarctic Pacific Ocean, Deep Sea Res. Part I Oceanogr. Res. Pap., 136, 107–118, 2018.

Table 1: Daily-integrated mixed layer net primary production (NPP) and net community production (NCP), including all components used to calculate NCP using $\Delta O_2/Ar$ or POC time series, as indicated: gross primary productivity (GPP), respiration (CR), vertical mixing (Mix), and gas exchange (J_{ex}). Derived POC export estimates assuming a maximum of 40% and 28% DOC/$NCP_{O2/Ar}$ during drifter periods 1 and 2, respectively, are provided, as well (Sects. 4.1.1, 4.1.3). All units here are in mmol C m^{-2} d^{-1}. Note that CbPM is the carbon-based production model (Sect. 2.5).

	Drifter 1:			**Drifter 2:**	
	Day 1	**Day 2**	**Day 3**	**Day 1**	**Day 2**
NPP (CbPM)	147 ± 61	137 ± 51	112 ± 40	22 ± 9	18 ± 7
NPP (^{14}C)	150 ± 18	-	49 ± 8	12 ± 4	-
GPP ($\Delta O_2/Ar$)	284 ± 75	270 ± 178	358 ± 198	108 ± 101	219 ± 211
GPP (POC)	242 ± 51	106 ± 26	98 ± 35	41 ± 8	38 ± 7
R ($\Delta O_2/Ar$)	-73 ± 65	-150 ± 88	-172 ± 56	-83 ± 35	-186 ± 64
R (POC)	-77 ± 55	-147 ± 28	-104 ± 40	-44 ± 12	-36 ± 9
Mix (N_2O)	70 ± 29	16 ± 81	19 ± 42	0	0
Mix (POC)	67 ± 47	12 ± 16	20 ± 16	0	0
J_{ex} (daily)	-62 ± 11	-7 ± 4	-6 ± 3	12 ± 5	17 ± 7
$NCP_{O2/Ar}$	140 ± 45	104 ± 84	167 ± 52	-12 ± 44*	33 ± 20
NCP_{POC}	97 ± 49	-53 ± 24	-25 ± 31	-2 ± 3	1 ± 2
POC export	0	115	126	0	23

*From three-hour increments of $NCP_{O2/Ar}$ (refer to Table 2). All other NCP values computed using day/night linear regressions of [POC] and $[O_2]_{bio}$ against time (Sects. 2.6.1, 2.6.2).

Table 2: Comparisons of NCP calculated using different time scales of integration (Sect. 2.6.3). For every calculation approach, "Export + DOC" is the average difference between $NCP_{O2/Ar}$ and NCP_{POC} values ± 1 S.D. or ± the propagated error. All units here are in mmol C m^{-2} d^{-1}.

	Drifter 1:					**Drifter 2:**		
	Day 1	**Day 2**	**Day 3**	**Mean ± S.D.**	**Export + DOC**	**Day 1**	**Day 2**	**Mean ± S.D.**
$NCP_{O2/Ar}$	140 ± 45	104 ± 84	167 ± 52	137 ± 32		26 ± 18	33 ± 20	29 ± 5
NCP_{POC}	97 ± 49	-53 ± 24	-25 ± 31	7 ± 80	131 ± 79	-2 ± 3	1 ± 2	-0.8 ± 3
$NCP_{O2/Ar}$ (3 hr)	177 ± 121	129 ± 102	122 ± 157	143 ± 30		-12 ± 44	25 ± 75	6 ± 26
NCP_{POC} (3 hr)	119 ± 66	-86 ± 64	53 ± 140	28 ± 105	115 ± 88	-8 ± 10	-6 ± 5	-7 ± 1
$NCP_{O2/Ar}$ (time points)	180 ± 54	128 ± 84	78 ± 43	129 ± 51		-4 ± 13	26 ± 11	11 ± 21
NCP_{POC} (time points)	99 ± 48	-73 ± 21	-14 ± 19	4 ± 87	124 ± 66	-6 ± 17	-2 ± 11	-4 ± 3
$NCP_{O2/Ar}$ (whole drifter trend)				103 ± 56				13 ± 9
NCP_{POC} (drifter trend)				-21 ± 28	121 ± 76			-4 ± 2

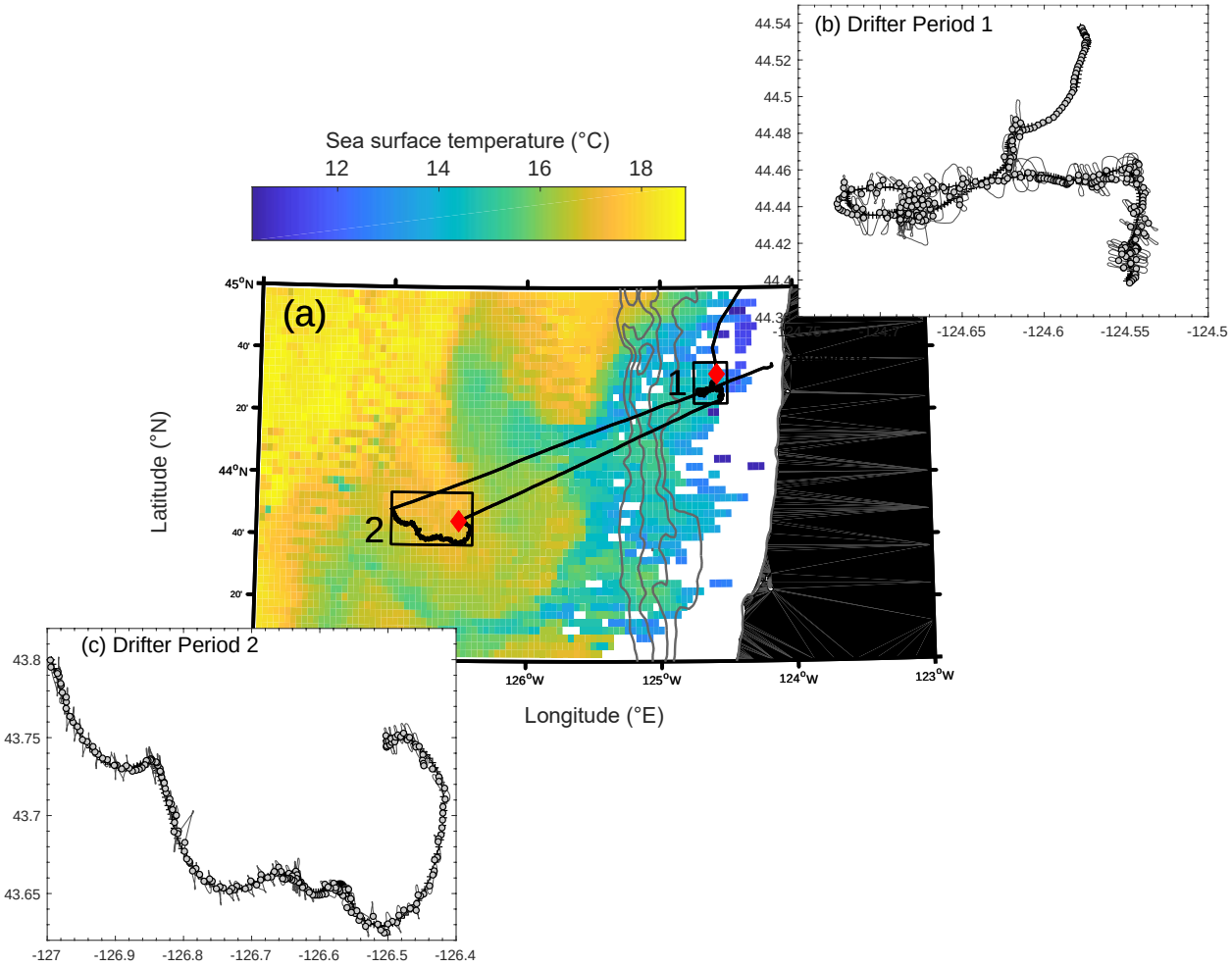

Figure 1: (a) Map of AQUA MODIS-derived 8-day composite sea surface temperature (11µm, nighttime) from 21-28 August 2017, overlapping with the duration of both drifter deployments. The two hollow boxes on the map denote location of drifter tracks, with the red diamonds indicating the location of the initial release. Gray bathymetry contours extend from 0-2000 m, with deepest contours representing the extent of the continental shelf. Panels (b and c) show a detailed view of the two drifter tracks, with the ship's track shown in a light grey line and circles denoting times when the ship was <1.5 km away from the drifter position. Only measurements taken at these cross-over locations were used for analysis.

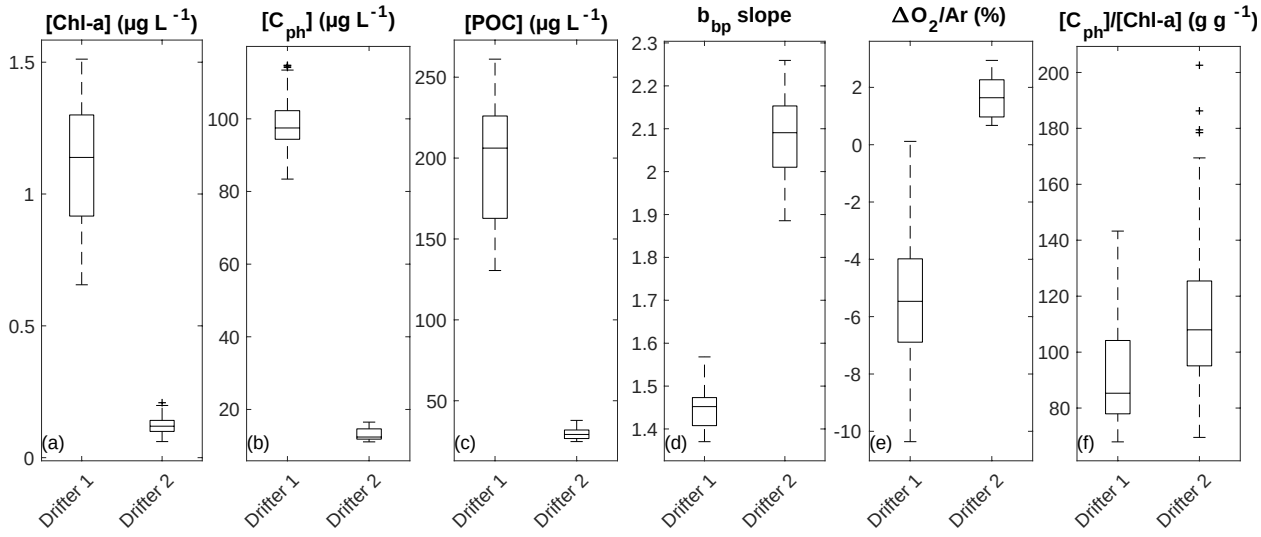

Figure 2: Comparison of average surface water properties between the two drifter deployments: (a) chlorophyll-a concentration (Chl-a), (b) phytoplankton carbon concentration (C_{ph}), (c) particulate organic carbon (POC) concentration, (d) the wavelength-dependent slope of particulate backscatter (b_{bp}), (e) biological oxygen saturation anomaly ($\Delta O_2/Ar$), and (f) the $[C_{ph}]/[Chl\text{-}a]$ ratio. Boxes represent the median (center line) and 25 and 75 percentiles (box edges). Outliers are indicated as black "+" marks.

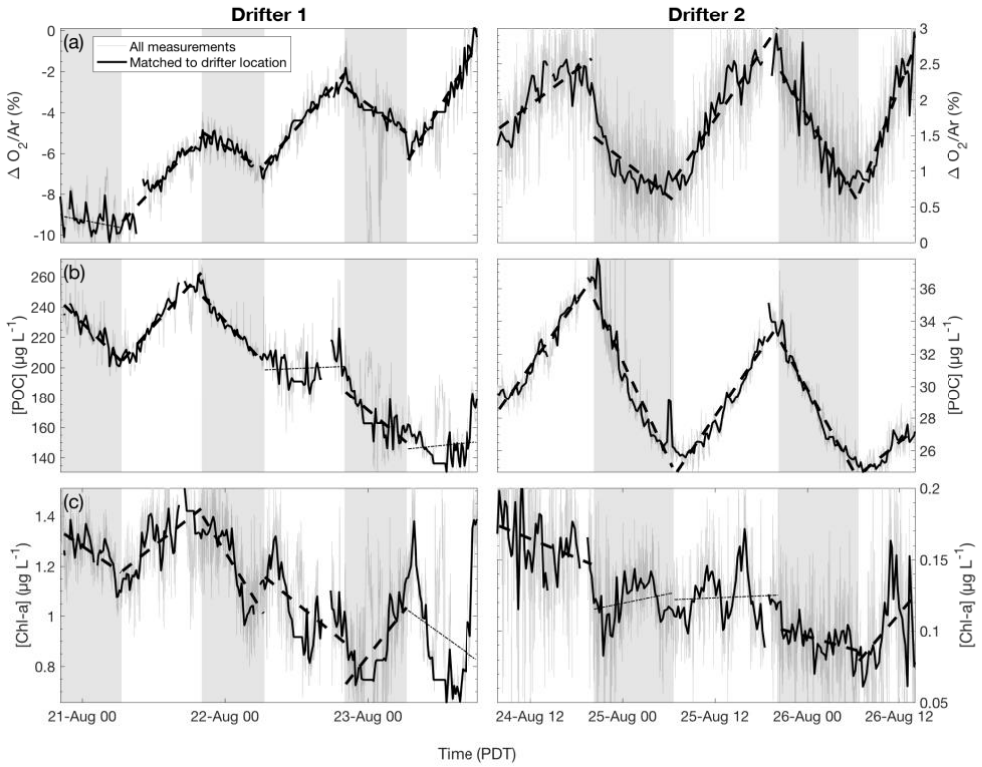

Figure 3: Time-series of (a) biological oxygen saturation ($\Delta O_2/Ar$), (b) particulate organic carbon (POC) concentration, and (c) chlorophyll-a (Chl-a) concentration during the two drifter deployments (left and right panels, respectively). For each daytime (non-shaded) and nighttime (shaded) interval, the best fit linear regression line is plotted. Significant regressions ($p<0.05$) are plotted as thick dashed lines, while non-significant regressions ($p\geq0.05$) are plotted as thin dotted lines. Grey lines show all measurements while thicker black line shows observations collected when the ship was within 1.5 km of the drifter location.

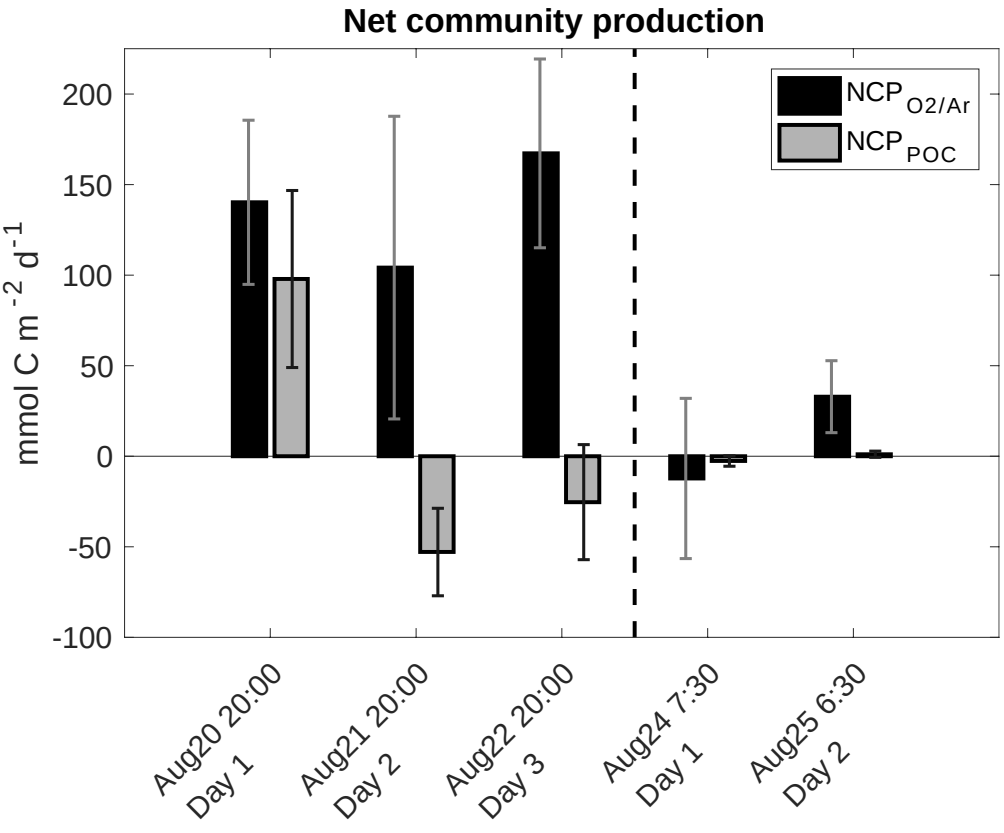

Figure 4: Daily net community production (NCP) during successive days of the two drifter deployments derived from diurnal variations of biological oxygen saturation ($\Delta O_2/Ar$), and particulate organic carbon (POC) concentration. Each set of bars is for one 24-hour period, with approximate starting times on the x-axis. Note that the negative $NCP_{O2/Ar}$ value for the first day of drifter period 2 was computed by integrating $NCP_{O2/Ar}$ values over eight consecutive three-hour increments (refer to Table 2).

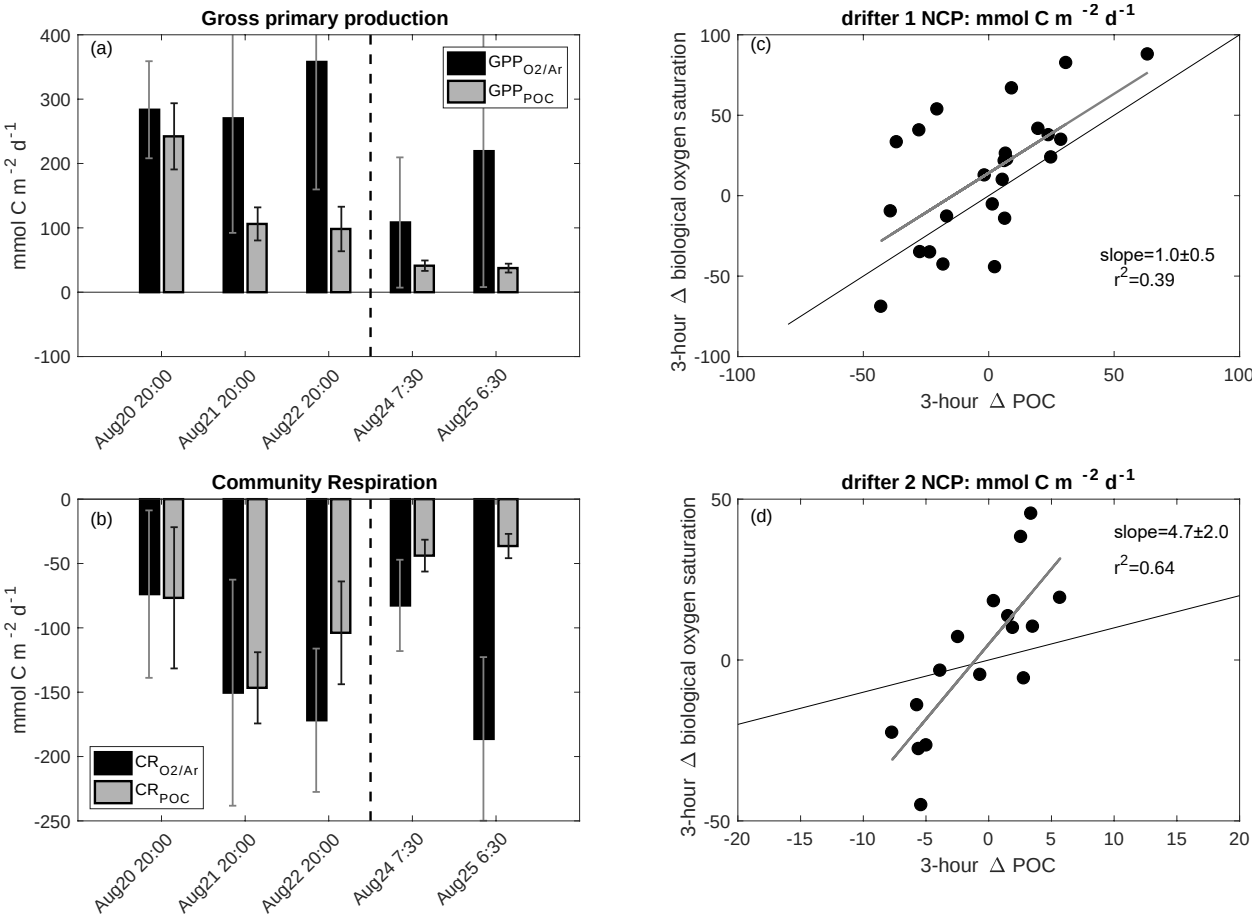

Figure 5: The left panels show comparisons between $\Delta O_2/Ar$-derived and POC-derived (a) GPP and (b) CR over the five days of both drifter deployments. The right panels show $\Delta O_2/Ar$-derived NCP ($NCP_{O2/Ar}$) as a function of POC-derived NCP (NCP_{POC}) over three-hour increments during (c) drifter period 1 and (d) drifter period 2. Thin black lines in (c) and (d) represent the 1:1 line, while thicker grey lines are the best-fit from linear regressions and correspond to the indicated slope and r_2 values.